Hydroformylation and tandem isomerization-hydroformylation of n-decenes using a rhodium-BiPhePhos catalyst: Kinetic modeling, reaction network analysis and optimal reaction control

Andreas Jörke[a,*], Tom Gaide[b], Arno Behr[b], Andreas Vorholt[b], Andreas Seidel-Morgenstern[a,c], Christof Hamel[a,d]

[a]*Otto von Guericke University, Magdeburg, Germany*
[b]*Technical University Dortmund, Dortmund, Germany*
[c]*Max Planck Institute for Dynamics of Complex Technical Systems, Magdeburg, Germany*
[d]*Anhalt University of Applied Sciences, Köthen, Germany*

Abstract

The rhodium-BiPhePhos catalyzed hydroformylation of n-decenes, as representative long-chain olefins, was investigated in this study experimentally and theoretically. Besides hydroformylation activity, the used catalyst enables significant double bond isomerization which is an essential side reaction. Because of this property, highly selective tandem isomerization-hydroformylation reactions that convert mixtures of n-decenes with internal double bond position to the desired terminal aldehyde undecanal are possible using the Rh-BiPhePhos catalyst. Experimentally, a reaction network analysis strategy was applied to study the coupled main and side reactions separately. Subsequently, a mechanistic kinetic model based on an extended Wilkinson-mechanism was developed that includes all relevant main and side reactions. Fitting the model to the 23 well planned experiments was possible with low deviations between model and experiment, including the tandem reaction. It was found that the tandem reaction shows completely opposite dependencies regarding temperature and synthesis gas pressure compared to the conventional hydroformylation of 1-decene, which is also covered by the model. Hence, strategies for optimal reaction performance of the (tandem isomerization-)hydroformylation were developed and presented.

Keywords: n-decene, Hydroformylation, Tandem reaction, Rhodium, BiPhePhos

1. Introduction

The homogeneously catalyzed addition of synthesis gas (carbon monoxide: CO and hydrogen: H_2) to the double bond of an olefin to produce aldehydes is known as hydroformylation for decades. It is one

*Corresponding author, email: andreas.joerke@ovgu.de, phone: +49-391-67-54655

of the most important homogeneously transition metal complex catalyzed reactions that is performed on industrial scales [1]. The addition of the formyl group in anti-Markovnikov position to an olefin double bond in terminal position yields the corresponding terminal aldehyde which is the desired product, whereas the branched aldehyde (Markovnikov product) is undesired because of lower market prices [2].
Mainly two metals, cobalt and rhodium, are used as hydroformylation catalysts [3]. Cobalt catalysts are cheap and robust but suffer from low activity. These drawbacks can be compensated with harsh reaction conditions. Milder reaction conditions can be applied, if the catalysis is performed with highly active but sensitive and expensive rhodium. Hence, Rh-catalysts are used increasingly in industry and research and therefore also in this study [2].
A wide range of mono- and diphosphorous ligands is available to modify Rh-catalysts for an improvement of activity and (regio)selectivity, such as phosphines [4–6], phosphonites [7, 8] and phosphites [9–13]. Recently, the chelating diphosphite ligand BiPhePhos (BP) [10] was studied in the literature intensively because of its capability of double bond isomerization of long-chain n-olefins and high hydroformylation regioselectivity towards linear aldehydes [14–20].
The double bond isomerization is a side reaction that reduces the overall linear aldehyde product yield, if n-olefins with terminal double bond position (terminal olefins) are used as substrates. The produced less reactive n-olefins with the double bond at internal positions (internal olefins) can undergo hydroformylation to undesired branched aldehydes [21]. On the other hand, the double bond isomerization activity of Rh-BiPhePhos catalysts can be exploited in challenging tandem isomerization-hydroformylation reactions to produce linear aldehydes from complex mixtures of internal olefins [14, 22–25]. From an industrial perspective, this is interesting because these feedstock types are cheap and available from e.g. cracking processes (internal butenes) and subsequent butene-dimerization (internal octenes) [21]. Another interesting application of tandem isomerization-hydroformylation reactions is the production of linear long-chain oxo-methylesters from green feedstocks, such as oleochemicals (e.g. ω-9 methyl oleate), that are platform chemicals for new types of bio-based polymers [26–30].
Proper reactor design for these new reactions requires a detailed mechanistic kinetic model including the main and all relevant side reactions. In particular, the double bond isomerization as a key reaction in tandem isomerization-hydroformylation systems has to be considered and included. The kinetic model should be able to describe all borderline cases between conventional hydroformylation of terminal olefins and tandem isomerization-hydroformylation of internal olefins. So far, no kinetic model can be found in the literature that satisfies these requirements. Thus, a new mechanistic kinetic model for

the Rh-BiPhePhos catalyzed (tandem isomerization-)hydroformylation of n-decenes, as representative long-chain olefins, was developed in this study. A reaction network analysis strategy [16, 17] was applied to decompose the coupled complex reaction system consisting of double bond isomerization, hydrogenation and hydroformylation to study these subnetworks separately. Corresponding time resolved (semi-)batch experiments were performed to estimate the kinetic parameters of the developed model, including the tandem isomerization-hydroformylation reaction, with complete resolution of all positional n-decene double bond isomers. The parameter estimation was supported by local parameter subset selection [31] to verify that the proposed experimental design is sufficient to achieve identifiability of the kinetic parameters. Based on the developed model, optimal reaction controls in terms of temperature and pressure profiles were calculated to maximize the aldehyde yield of the (tandem isomerization-)hydroformylation.

2. Reaction mechanisms

One generally accepted hydroformylation mechanism for cobalt and rhodium catalysts is the "Wilkinson" cycle (see figure 1) [4]. This mechanism was extended to take the most dominant side reactions (double bond isomerization, hydrogenation and iso-aldehyde production) into account [16, 17]. The mechanism can be divided into two parts: (1) the catalyst formation and pre-equilibrium and (2) the coupled reaction cycles consisting of double bond isomerization (branch **I**), double bond hydrogenation (branch **IIa-b**) and hydroformylation (branch **IIIa** for the production of linear aldehydes and **IIIb** for the production of branched aldehydes).

Operando FTIR spectroscopy was used in the literature to study the catalyst pre-equilibrium and the hydroformylation reaction using a Rh-BiPhePhos catalyst and 1-decene as substrate [32]. It was found that the activated $HRh(BP)(CO)_2$ complex was formed rapidly even at low temperature (40 °C) in two steps: (1) Adding the ligand to the Rh-precursor $Rh(acac)(CO)_2$ yielded a Rh(acac)(BP) complex under release of CO and (2) addition of synthesis gas to Rh(acac)(BP) under release of acac-H gave the saturated 18ve Rh-hydridodicarbonyl complex $HRh(BP)(CO)_2$, exclusively. Under hydroformylation conditions using the BiPhePhos ligand, this complex was the only detectable Rh-species over almost complete olefin conversion [32]. Therefore, the formation of saturated acyl complexes, Rh-clusters and other inactive Rh-species that may be formed under low H_2 pressure were neglected in this study as a first approximation.

In the case of hydroformylation, the olefin coordinates at the unsaturated and active 16ve Rh-hydrido-carbonyl complex HRh(BP)(CO) (resting state RS) and the double bond is inserted into the Rh-hydride

bond. Which sp^2 carbon is inserted decides whether a linear or a branched aldehyde is formed (branch **IIIa** or **IIIb**). After addition and migratory insertion of CO into the alkyl substituent to form an unsaturated acyl complex, oxidative H_2 addition occurs and changes the oxidation state of Rh from +1 to +3. The reductive elimination releases the aldehyde, reduces the oxidation state of Rh back to +1 and the active 16ve resting state is formed back again to close the catalytic cycle. It is assumed that the oxidative addition of H_2 and the reductive elimination steps to release the product (alkane, aldehyde) are irreversible [12, 33, 34]. The hydrogenation proceeds similarly but without addition and migratory insertion of CO because the oxidative H_2 addition comes first (branch **IIa-b**). The oxidative addition of H_2 to HRh(BP)(CO) forming the Rh(III) species H_3Rh(BP)(CO) under hydrogenation conditions was, however, not considered in this work. If β-H elimination follows the double bond insertion, internal olefins are produced until the thermodynamic equilibrium composition of the internal olefins is reached (subnetwork **I**) [19, 20, 35].

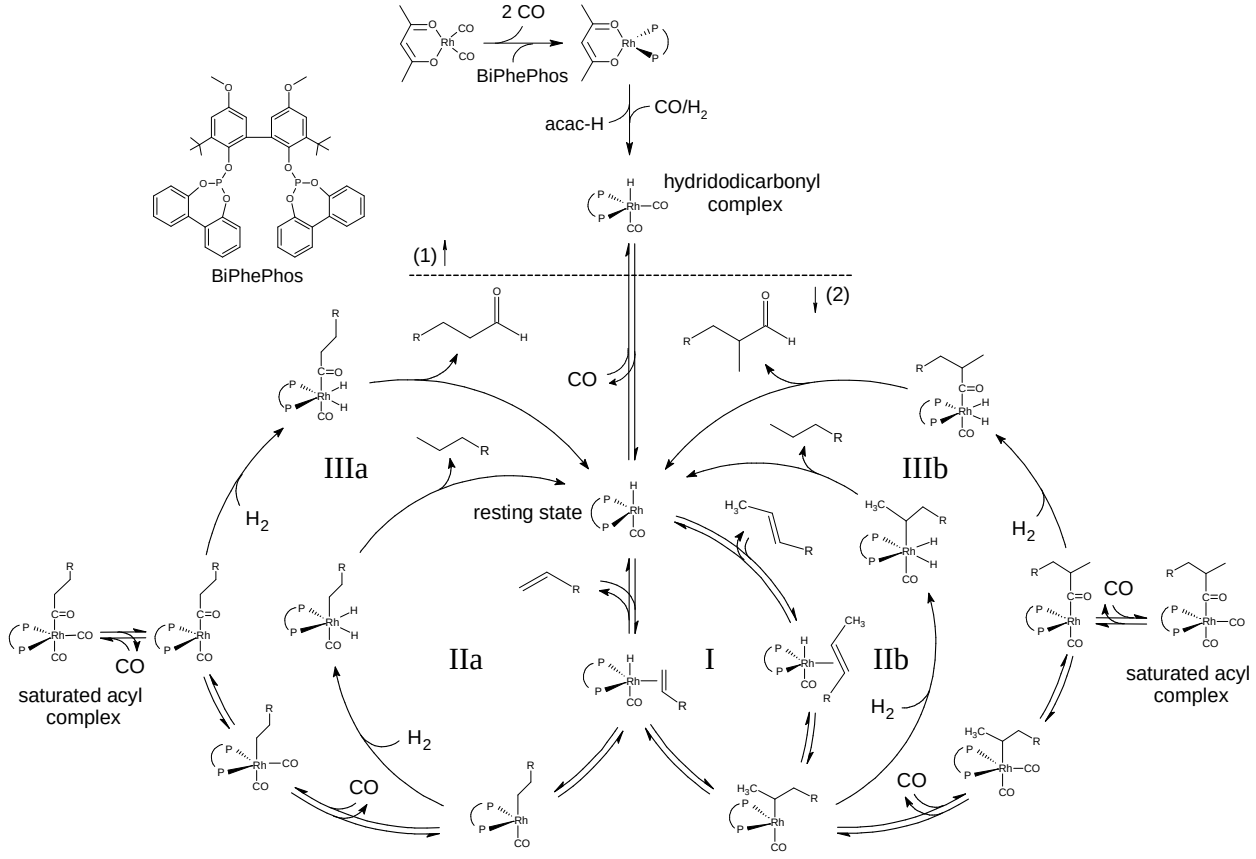

Figure 1: Extended Rh-BiPhePhos catalyzed hydroformylation reaction mechanism including the catalyst pre-equilibrium, main and side reactions: **I** double bond isomerization, **IIa-b** olefin hydrogenation and **IIIa-b** olefin hydroformylation to produce linear and branched aldehydes, respectively.

The mechanism of the tandem isomerization-hydroformylation of n-olefin mixtures with internal double bond consists of two simultaneous steps. First, the hydroformylation reaction (branch **IIIa** in figure 1) consumes terminal olefins from the olefin mixture at thermodynamic equilibrium and disturbs the latter. At the same time, the fast equilibrium controlled isomerization reaction (branch **I** in figure 1) works against this disturbance to restore the thermodynamic equilibrium. In this manner, new terminal olefins from internal olefins are produced which are then available for hydroformylation again [25].

3. Experimental section and reaction network analysis

Since all branches in the extended mechanism discussed above run in parallel, it is difficult to study them separately. Therefore, the complex system was divided into three major subnetworks (isomerization, hydrogenation and hydroformylation) and decoupled experimentally. Controlling which reaction takes place is possible by manipulating the gas phase composition. This can be done by gas phase exchange after activation of the catalyst with synthesis gas. The individual subnetworks were studied successively with increasing complexity (isomerization $<$ hydrogenation $<$ hydroformylation). This procedure is explained in detail for the individual subnetworks in the subsequent paragraphs.

All experiments were performed in a high pressure multi-reactor system (Parr Instrument Co.) using 75 ml liquid volume (semi)batch autoclaves equipped with a pressure lock for substrate injection. The used equipment was identical to our previous studies and is explained in detail in the literature [19, 20].

Quantitative analysis of the composition of reaction mixture samples was performed using an Agilent 6890 series gas chromatograph (GC) equipped with a flame ionization detector (FID). Two GC columns were used in this study: (1) HP-5, 5% phenyl 95% methylpolysiloxan, length 30 m, diameter 0.25 mm, film: 0.25 μm and (2) HP-INNOWax, polyethylene glycol, length: 120 m, diameter: 0.25 mm, film: 0.25 μm. The first column enables fast analysis and a good resolution of the reactants and products (for details and example chromatogram see [19]). However, this column has limited resolution of the n-decene isomers. Therefore, the second column was used additionally to achieve complete resolution of all n-decene isomers for selected experiments because of long analysis times (for details and example chromatogram see [20]). The experiments that were analyzed with the second column to achieve complete n-decene isomer resolution are labeled with a star in the following table 1 that summarizes the experimental design. GC calibration was performed with commercially available high purity calibration standards of the reactants and products including all n-decene isomers (ChemSampCo, ABCR, Sigma-Aldrich). However, it was not possible to identify all possible branched iso-aldehydes. Therefore, the suspected iso-aldehyde

peaks were lumped and denoted as "iso-aldehyde". Dodecane as part of the solvent system, which is explained in the following section, was used as internal standard.

3.1. Solvent

The used solvent is a thermomorphic multicomponent solvent system (TMS) [36, 37]. This solvent mixture is completely homogeneous at high reaction temperature and heterogeneous (2 liquid phases, polar and non-polar) at low temperatures. Since the precious metal catalyst is dissolved preferentially in the polar phase while the reactants remain in the non-polar phase, this concept enables stable and energy efficient catalyst recycling over multiple runs [15, 38]. The TMS consists of dimethylformamide (dmf, Merck $>$ 99 %) as polar solvent, dodecane (dod, Alfa Aesar $>$ 99 %) as non-polar solvent, and mixtures of 1-decene (1D, Sigma Aldrich 94 %) and iso-decene (iD, Sasol, technical mixture of all possible n-decene isomers at thermodynamic equilibrium, composition: see [19]) as substrates. The composition of the TMS (n-decene:dod:dmf = 1:3:4 molar) represents an equimolar ratio between polar and non-polar molecules and becomes homogeneous at 85 °C.

3.2. Catalyst activation

To activate the catalyst, the Rh-precursor Rh(acac)$(CO)_2$ and the ligand BiPhePhos were dissolved in dmf and dodecane at room temperature. The mixture was added to the reactor and inertized under stirring with Schlenk technique using nitrogen. Applying a synthesis gas atmosphere ($CO:H_2$ = 1:1, isomerization/hydrogenation: 15 bar, hydroformylation: $\approx$ 2 bar less than reaction pressure) while heating up the mixture to reaction temperature (95 - 135 °C, ca. 30 min) under constant stirring (1200 rpm) initiated the formation of saturated 18ve Rh-hydridodicarbonyl complexes HRh(BP)$(CO)_2$.

3.3. Isomerization

To perform isomerization reactions without hydrogenation or hydroformylation, the synthesis gas atmosphere was removed completely after the catalyst activation. Cooling down the reactor to room temperature before removing the gas phase using a vacuum pump and inert nitrogen for flushing is necessary to avoid evaporation of the solvents. Subsequent n-olefin injection into the solvent-catalyst mixture via the pressure lock with inert pressurized nitrogen or CO starts the isomerization reaction. Using CO as injection gas allows to study the CO dependence of the equilibrium between the inactive 18ve hydridodicarbonyl complex HRh(BP)$(CO)_2$ and the active 16ve hydridocarbonyl complex HRh(BP)(CO) indirectly. This

is possible, because the isomerization reaction itself is not influenced by CO (see figure 1). Thus, a CO induced change in isomerization reaction rate has to originate from the formation of inactive $HRh(BP)(CO)_2$ which reduces the overall available amount of active catalyst. In total, 6 isomerization experiments were performed. The experimental conditions, initial pressures and initial molar ratios are summarized in table 1. At CO pressures below 2 bar, additional 2 bar of inert nitrogen was added to allow liquid sampling. In all other cases, the partial pressure of CO is identical to the total pressure.

3.4. Hydrogenation

The hydrogenation subnetwork was analyzed by removing synthesis gas after the catalyst activation and replacing it with pure H_2. The applied H_2 pressure before substrate injection was set to 1-2 bar below the initial hydrogenation pressure to keep the catalyst close to the desired reaction conditions. Different feed mixtures, including the hydrogenation product decane, were hydrogenated to study if the components are influencing each other. In total, 4 hydrogenation experiments were performed. The experimental conditions, initial H_2 pressures and initial molar ratios are summarized in table 1. It should be noted that these experiments include the double bond isomerization as side reaction.

3.5. Hydroformylation

Performing hydroformylation reactions does not require to exchange the gas phase after catalyst activation. Using 1-decene and a technical equilibrium mixture of all n-decene isomers in different feed ratios allowed to study the coupling between isomerization and hydroformylation. Since the tandem isomerization-hydroformylation reaction is slow, the reaction temperature and the catalyst loading were increased up to 135 °C and a Rh:substrate ratio of 1:500, respectively, which marks the upper limit of catalyst stability [38]. In total, 8 hydroformylation and 5 tandem isomerization-hydroformylation experiments were performed, whereas the iHyfo 5 experiment represents optimized reaction conditions applied in [38] where the reaction system was developed. The experimental conditions, initial synthesis gas pressures and initial molar ratios are summarized in table 1. It should be noted that the hydroformylation experiments include all side reactions (isomerization, hydrogenation, iso-aldehyde formation), which underlines the necessity of applying the successive reaction network analysis.

Table 1: Experimental design for subnetwork analysis: Isomerizatrion, Hydrogenation, Hydroformylation and tandem isomerization-hydroformylation. Initial concentration of n-decene: 0.9 mol l^{-1} (except iHyf 5: 1.2 mol l^{-1}).

Exp. ID	$p_{CO/H2}$ / bar	T / °C	1D:iD	Rh:Substrate	Rh:BP	Gas supply
Iso 1*	0.00	105	1:0	1:10000	1:3	No consumption
Iso 2	0.84	105	1:1	1:10000	1:3	No consumption
Iso 3	4.90	105	1:0	1:10000	1:3	No consumption
Iso 4	9.62	105	1:0	1:10000	1:3	No consumption
Iso 5	5.93	95	1:0	1:10000	1:3	No consumption
Iso 6	6.45	115	1:0	1:10000	1:3	No consumption
Hyd 1	20.48	105	3:1:0	1:10000	1:3	batch
Hyd 2	21.11	105	0:4:3	1:10000	1:3	batch
Hyd 3	10.72	95	0:1:0	1:10000	1:3	batch
Hyd 4	10.58	115	0:1:0	1:10000	1:3	batch
Hyfo 1	6.00	105	1:0	1:10000	1:3	batch
Hyfo 2	11.33	105	1:0	1:10000	1:3	batch
Hyfo 3	22.44	105	1:0	1:10000	1:3	batch
Hyfo 4	21.67	105	1:1	1:10000	1:3	batch
Hyfo 5	6.81	105	7:4	1:10000	1:3	batch
Hyfo 6	6.02	105	2:9	1:10000	1:3	batch
Hyfo 7	21.11	115	1:0	1:10000	1:3	batch
Hyfo 8	21.95	95	1:0	1:10000	1:3	batch
iHyfo 1*	5.34	105	0:1	1:1000	1:3	semibatch
iHyfo 2	10.50	105	0:1	1:1000	1:3	semibatch
iHyfo 3*	21.09	105	0:1	1:1000	1:3	semibatch
iHyfo 4*	5.08	135	0:1	1:1000	1:5	semibatch
iHyfo 5*	5.11	135	0:1	1:500	1:5	semibatch

4. Kinetic modeling

The subnetwork analysis discussed above focuses on three major reactions: the double bond isomerization, hydrogenation and hydroformylation. It is intended in this chapter to assign a mechanistic kinetic model to each corresponding reaction. Nevertheless, the complex reaction mechanism has to be simplified. For the isomerization case, only the shift of the double bond position was considered. This corresponds to lumped cis and trans isomers and sums up in total to 4 equilibrium limited reaction rate laws. For the hydrogenation case, it is assumed that terminal olefins are hydrogenated much faster than internal olefins due to less steric hindrances (see [2] and section 5.1 in this work). Therefore, the branch **IIb** in figure 1 was neglected and only one reaction rate model is needed for the hydrogenation of 1-decene to decane. For the hydroformylation case, it is assumed that terminal decenes can be converted to the desired linear aldehyde (anti-Markovnikov addition) but also to the undesired branched aldehyde (Markovnikov addition). This corresponds to two reaction rate laws. Additionally, internal olefins can also be converted to "iso-aldehydes". However, it was also not possible to decide which internal olefin was converted to

which "iso-aldehyde". Therefore, a third rate law was set up that represents the transformation of the sum of all internal olefins to the pseudo-component "iso-aldehyde". The simplified reaction network presented in figure 2 illustrates these assumptions.

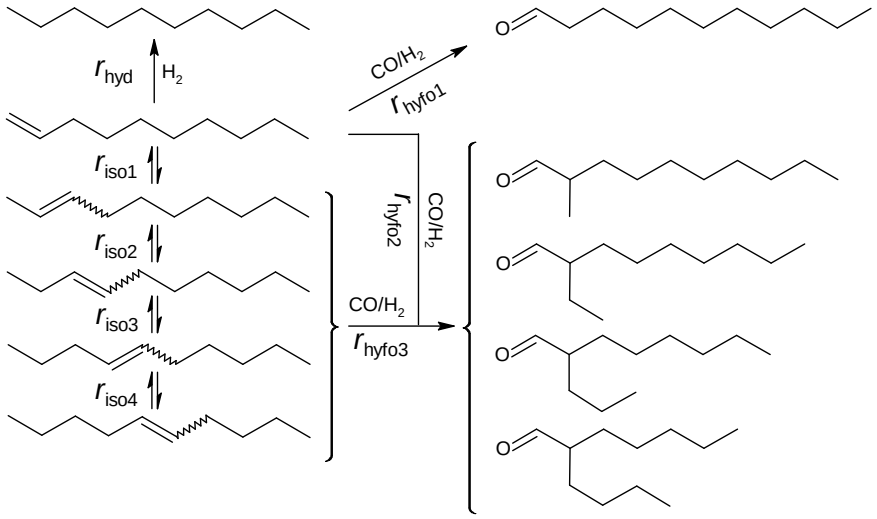

Figure 2: Proposed reaction network including all main and side reactions. The corresponding kinetic models for the reaction rates r are summarized in table 2.

The mechanistic kinetic modeling of the discussed reactions followed Christiansen's method in this contribution [39]. This method applies Bodensteins's principle [40] to a steady state catalytic cycle or sequence with n steps. It is assumed that the concentration of catalytic intermediates remains at trace level and that all steps involve maximum one catalytic intermediate as reactant to make use of linear algebra. For details about the cumbersome derivation of the method's equations, we refer to the literature [39, 41, 42]. The central quantities of this method are pseudo first order rate coefficients λ_{ij} for a reaction of a catalytic intermediate i to intermediate j. These pseudo first order rate coefficients are the product of a pseudo-rate constant and the concentrations of reactants that enter the catalytic cycle or sequence. The pseudo rate constant is, in turn, the product of the rate constant of an elementary step and the constant concentration of the catalyst intermediate that drives the elementary reaction (Bodenstein approximation). Per convention, the starting intermediate of the catalytic cycle or sequence (resting state) is denoted with index $= 1$ which is the HRh(BP)(CO) complex in our case. All following intermediates are numbered continuously (see equation (1)). The derivation of the mechanistic reaction rate law for the hydroformylation of 1-decene to undecanal r_{hyfo1} is explained in the following as an example. All other rate laws were derived analogously. The pseudo-first order rate coefficients λ_{ij} for Hydroformylation 1

(branch **IIIa** in figure 1) are:

$$\begin{aligned} \lambda_{12} &= k_{12} c_{1D} & \lambda_{21} &= k_{21} \\ \lambda_{23} &= k_{23} & \lambda_{32} &= k_{32} \\ \lambda_{34} &= k_{34} c_{CO} & \lambda_{43} &= k_{43} \\ \lambda_{45} &= k_{45} & \lambda_{54} &= k_{54} \\ \lambda_{56} &= k_{56} c_{H2} & \lambda_{65} &= 0 \\ \lambda_{61} &= k_{61} & \lambda_{16} &= 0. \end{aligned} \tag{1}$$

λ_{65} and λ_{16} are zero because the corresponding reactions between complexes 1, 5 and 6 are assumed to be irreversible. The general expression of the reaction rate r for a catalytic reaction cycle is given by the method in the literature by equation (2) [39, 41, 42].

$$r = \frac{\left(\prod_{i=1}^{n-1} \lambda_{i(i+1)} \lambda_{n1} - \prod_{i=1}^{n-1} \lambda_{(i+1)i} \lambda_{1n} \right) c_{RS}}{\sum_i \sum_j \mathbf{C}_{ij}} \tag{2}$$

If several catalytic cycles are running in parallel, as it is the case in this study, it is possible that they have an influence on each other, which makes the kinetic modeling very complicated. However, considering the reaction cycles as independent from each other to use equation (2) is possible, if the majority of the catalyst material is located at the starting point (resting state) of the cycles and not within a cycle [41]. Since the Rh-hydridodicarbonyl complex HRh(BP)$(CO)_2$ (HDC) was observed experimentally with operando FTIR spectroscopy as the dominant Rh-intermediate under hydroformylation conditions using the Rh-BiPhePhos catalyst [32], it is likely that most of the Rh is present as HRh(BP)$(CO)_2$ and HRh(BP)(CO), which are at equilibrium with each other (see figure 1). This observation justifies the usage of equation (2) because the resting state concentration c_{RS} in equation (2) belongs to this Rh-hydridocarbonyl complex HRh(BP)(CO).

The equilibrium assumption between HRh(BP)$(CO)_2$ and HRh(BP)(CO) is equivalent with a fast dissociation of CO. This is reasonable for phosphite ligands, because CO and the phosphite compete with each other for π-backbonding at the Rh-center which weakens the Rh-CO bond [1, 2, 43, 44]. Hence, the concentration of the hydridocarbonyl complex HRh(BP)(CO) can be calculated from the Rh-balance (3) and the mass action law of the equilibrium between those complexes (4). The total amount of Rh is equal

to the amount of used catalyst precursor Rh(acac)$(CO)_2$ (PC).

$$c_{\mathrm{PC}} = c_{\mathrm{HDC}} + c_{\mathrm{RS}} \tag{3}$$

$$K_{\mathrm{cat}} = \frac{c_{\mathrm{HDC}}}{c_{\mathrm{RS}} c_{\mathrm{CO}}} \tag{4}$$

Combining equations (3) and (4) gives the catalyst resting state concentration as a function of the catalyst precursor and CO concentration:

$$c_{\mathrm{RS}} = \frac{c_{\mathrm{PC}}}{(1 + K_{\mathrm{cat}} c_{\mathrm{CO}})}. \tag{5}$$

The square Christiansen matrix $\mathbb{C}$ in equation (2) contains permutations of the pseudo-first order rate coefficients λ_{ij} of all forward and backward elementary reactions and the stoichiometric number ν_i of each step (= 1 in our case). Generally, $\mathbb{C}$ for a catalytic cycle with n intermediates and steps is given by

$$\mathbb{C} = \begin{pmatrix} \nu_1\lambda_{23}\lambda_{34}\ldots\lambda_{n1} & \lambda_{21}\nu_2\lambda_{34}\ldots\lambda_{n1} & \cdots & \lambda_{21}\lambda_{32}\lambda_{43}\ldots\nu_n \\ \lambda_{12}\nu_2\lambda_{34}\ldots\lambda_{n1} & \lambda_{12}\lambda_{32}\nu_3\ldots\lambda_{n1} & \cdots & \nu_1\lambda_{32}\lambda_{43}\ldots\lambda_{1n} \\ \cdots & \cdots & \cdots & \cdots \\ \lambda_{12}\lambda_{23}\lambda_{34}\ldots\nu_n & \nu_1\lambda_{23}\lambda_{34}\ldots\lambda_{1n} & \cdots & \lambda_{21}\lambda_{32}\ldots\nu_{n-1}\lambda_{1n} \end{pmatrix}. \tag{6}$$

Including the assumptions of irreversible oxidative H_2 addition and reductive elimination discussed in section 2 (λ_{65} and $\lambda_{16} = 0$), the Christiansen matrix of Hydroformylation 1 becomes:

$$\mathbb{C}_{\mathrm{hyfo}} = \begin{pmatrix} \lambda_{23}\lambda_{34}\lambda_{45}\lambda_{56}\lambda_{61} & \lambda_{21}\lambda_{34}\lambda_{45}\lambda_{56}\lambda_{61} & \lambda_{21}\lambda_{32}\lambda_{45}\lambda_{56}\lambda_{61} & \lambda_{21}\lambda_{32}\lambda_{43}\lambda_{56}\lambda_{61} & \lambda_{21}\lambda_{32}\lambda_{43}\lambda_{54}\lambda_{61} & 0 \\ \lambda_{12}\lambda_{34}\lambda_{45}\lambda_{56}\lambda_{61} & \lambda_{12}\lambda_{32}\lambda_{45}\lambda_{56}\lambda_{61} & \lambda_{12}\lambda_{32}\lambda_{43}\lambda_{56}\lambda_{61} & \lambda_{12}\lambda_{32}\lambda_{43}\lambda_{54}\lambda_{61} & 0 & 0 \\ \lambda_{12}\lambda_{23}\lambda_{45}\lambda_{56}\lambda_{61} & \lambda_{12}\lambda_{23}\lambda_{43}\lambda_{56}\lambda_{61} & \lambda_{12}\lambda_{23}\lambda_{43}\lambda_{54}\lambda_{61} & 0 & 0 & 0 \\ \lambda_{12}\lambda_{23}\lambda_{34}\lambda_{56}\lambda_{61} & \lambda_{12}\lambda_{23}\lambda_{34}\lambda_{54}\lambda_{61} & 0 & 0 & 0 & 0 \\ \lambda_{12}\lambda_{23}\lambda_{34}\lambda_{45}\lambda_{61} & 0 & 0 & 0 & 0 & 0 \\ \lambda_{12}\lambda_{23}\lambda_{34}\lambda_{45}\lambda_{56} & 0 & 0 & 0 & 0 & 0 \end{pmatrix}. \tag{7}$$

Further reasonable simplification of the Christiansen matrix is possible, if a rate determining step in the cycle is assumed. The coordination of the olefin to the hydridocarbonyl complex HRh(BP)(CO) is likely to be the rate determining step [32]. Therefore, all entries in the Christiansen matrix that contain the olefin

coordination step λ_{12} were neglected:

$$\mathbb{C}_{\text{hyfo}} = \begin{pmatrix} \lambda_{23}\lambda_{34}\lambda_{45}\lambda_{56}\lambda_{61} & \lambda_{21}\lambda_{34}\lambda_{45}\lambda_{56}\lambda_{61} & \lambda_{21}\lambda_{32}\lambda_{45}\lambda_{56}\lambda_{61} & \lambda_{21}\lambda_{32}\lambda_{43}\lambda_{56}\lambda_{61} & \lambda_{21}\lambda_{32}\lambda_{43}\lambda_{54}\lambda_{61} & 0 \\ 0 & 0 & 0 & 0 & 0 & 0 \\ 0 & 0 & 0 & 0 & 0 & 0 \\ 0 & 0 & 0 & 0 & 0 & 0 \\ 0 & 0 & 0 & 0 & 0 & 0 \\ 0 & 0 & 0 & 0 & 0 & 0 \end{pmatrix}. \quad (8)$$

With the summation over all entries in $\mathbb{C}_{\text{hyfo}}$, together with equation (2) and (5), follows the hydroformylation rate law for the production of undecanal from 1-decene:

$$r_{\text{hyfo1}} = \frac{k_{12}k_{23}k_{34}k_{45}k_{56}k_{61}c_{1\text{D}}c_{\text{CO}}c_{\text{H2}}}{\begin{array}{c} k_{21}k_{32}k_{43}k_{54}k_{61} + \left(k_{21}k_{32}k_{45}k_{56}k_{61} + k_{21}k_{32}k_{43}k_{56}k_{61}\right)c_{\text{H2}} + \\ \left(k_{23}k_{34}k_{45}k_{56}k_{61} + k_{21}k_{34}k_{45}k_{56}k_{61}\right)c_{\text{H2}}c_{\text{CO}} \end{array}} \cdot \frac{c_{\text{PC}}}{\left(1 + K_{\text{cat}}c_{\text{CO}}\right)}. \quad (9)$$

The derivation of the other rate laws assumed the olefin coordination as rate determining step as well. Double bond isomerization of 1-decene to lumped positional (cis+trans) n-decene isomers, the hydrogenation of 1-decene to decane and the production of iso-aldehydes from 1-decene and all internal decenes were considered as major side reactions.

For simplification and parameter space reduction, the temperature dependence of the reaction rates is represented by the apparent rate constant while the inhibition parameters in the denominator were assumed to be temperature independent. The temperature dependent rate constants $k(T)$ were modeled using a reparameterized Arrhenius approach (10) to avoid correlations between the apparent collision factor k_{inf} and the apparent activation energy E_{A} [45, 46]. The latter can be recalculated from the coefficients A and B of equation (10) using equations (11) and (12) (reference temperature $T_{\text{ref}} = 105\ ^{\circ}\text{C}$).

$$k(T) = \exp\left(A + B\left(1 - \frac{T_{\text{ref}}}{T}\right)\right) \quad (10)$$

$$k_{\text{inf}} = \exp(A + B) \quad (11)$$

$$E_{\text{A}} = B \cdot RT_{\text{ref}} \quad (12)$$

The inhibition parameters of Hydroformylation 1 are different to Hydroformylation 2 and 3 , because they belong to different branches in the catalytic cycle (branch **IIIa** vs. **IIIb**). It is therefore very likely that they have different values. Additionally, it is assumed that the apparent activation energies of the

double bond isomerization of internal decenes are similar ($B_{\mathrm{iso2}} = B_{\mathrm{iso3}} = B_{\mathrm{iso4}}$) and that the apparent activation energies of the production of iso-aldehydes are similar ($B_{\mathrm{hyfo2}} = B_{\mathrm{hyfo3}}$) to reduce the number of parameters that have to be estimated. The isomerization equilibrium constants $K_{\mathrm{iso1-4}}$ are given by Benson's group contribution method predictions in the literature [19] and were evaluated at the mean temperature of the studied temperature range (115 °C) because of their minor temperature dependence (see table 2). In total 19 kinetic parameters have to be estimated. All parameters are identifiable and can be estimated with the proposed experimental design, which was verified by the method of local parameter subset selection [31] (see Appendix A). Table 2 summarizes all derived rate laws with lumped elementary step rate constants as well as the corresponding estimated parameter values with 95 % confidence interval.

5. Experimental results and parameter estimation

The parameter estimation was performed by minimizing the difference between measurements from (semi)batch experiments and a (semi)batch reactor model using Matlab 2012a with a standard nonlinear least-squares solver (lsqnonlin) and central differences for gradient approximation. All experiments were evaluated simultaneously to estimate the model parameter vector as a whole and no sequential fitting procedure was used. However, the individual subnetworks are discussed separately below. Details about the underlying reactor model and experimentally determined gas solubilities can be found in the literature [31].

5.1. Isomerization

The experimentally determined and time resolved concentration profiles of the isomerization of 1-decene to internal decenes (in accordance to table 1) are presented in figure 4 as well as the corresponding modeling results. The estimated kinetic parameters for the catalyst pre-equilibrium and the isomerization rates are summarized in table 2. The experimental results show a strong dependence of the double bond isomerization on the applied CO partial pressure. Already low CO partial pressures (Iso 2) inhibit the isomerization reaction significantly. At higher partial pressures of CO above 5 bar (Iso 3-6), no significant isomerization of 1-decene beyond the formation of 2-decenes was observable, indicating a strong reduction of the catalyst activity. Without CO, however, the catalyst activity is high and even the most internal double bond isomers were formed until the reaction equilibrium was reached (Iso 1) in a series reaction sequence (figure 2). The observed reaction rate reduction is assigned to the CO induced formation of the coordinationally saturated 18ve $HRh(BP)(CO)_2$ complex, reducing the amount of active

16ve HRh(BP)(CO). Figure 3 shows the amount of active 16ve HRh(BP)(CO) relative to the total Rh amount in percent calculated with equation (5) and the estimated value for K_{cat}. Already low CO partial pressures of 2 bar reduce the relative amount of active catalyst material below 1 %. Hence, the catalyst pre-equilibrium is, of course, strongly on the side of the 18ve HRh(BP)$(CO)_2$ with noble gas configuration which affects all reactions. A very similar trend was found using a TDTBPP ligand in twenty-fold excess [47].

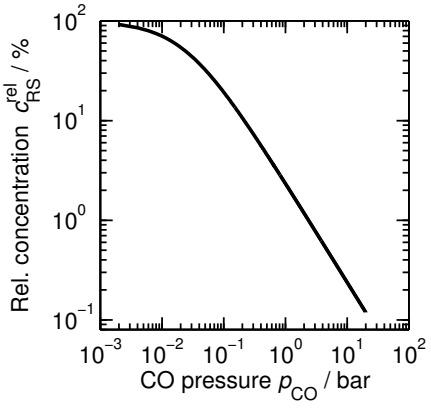

Figure 3: Relative resting state concentration c_{RS}/c_{PC} in % as a function of CO partial pressure at 115 °C (equation (5)). The gas solubility of CO to calculate the corresponding liquid phase concentration of CO was experimentally determined in the literature for the used TMS [31].

Furthermore, it can be seen from the experimental data (Iso 1) that the isomerization rates slowed down with more internal double bond position. The corresponding relative isomerization rate constants at reference temperature are $k_{iso1} : k_{iso2} : k_{iso3} : k_{iso4} = 161.2 : 2.7 : 2.7 : 1$ (see table 2). This is a consequence of stronger steric hindrances for the coordination of the internal olefins to the Rh-catalyst compared to the terminal olefin because the olefin coordination is rate determining.

The developed mechanistic kinetic model (equations (13-16)) fits the experimental data very well with only two estimated parameters per isomerization reaction and one parameter controlling the catalyst pre-equilibrium. This emphasizes the advantage of mechanistic kinetic expressions and supports the assumption that the olefin coordination is also the rate determining step for the double bond isomerization. The high catalyst activity under absence of H_2 and the fact that the kinetic model for the isomerization reactions works equally good under pure H_2 or synthesis gas atmosphere with the same kinetic parameter values (see section 5.2 and 5.3), supports the assumption that the formation of inactive Rh-dimers can be neglected for the used conditions and ligand.

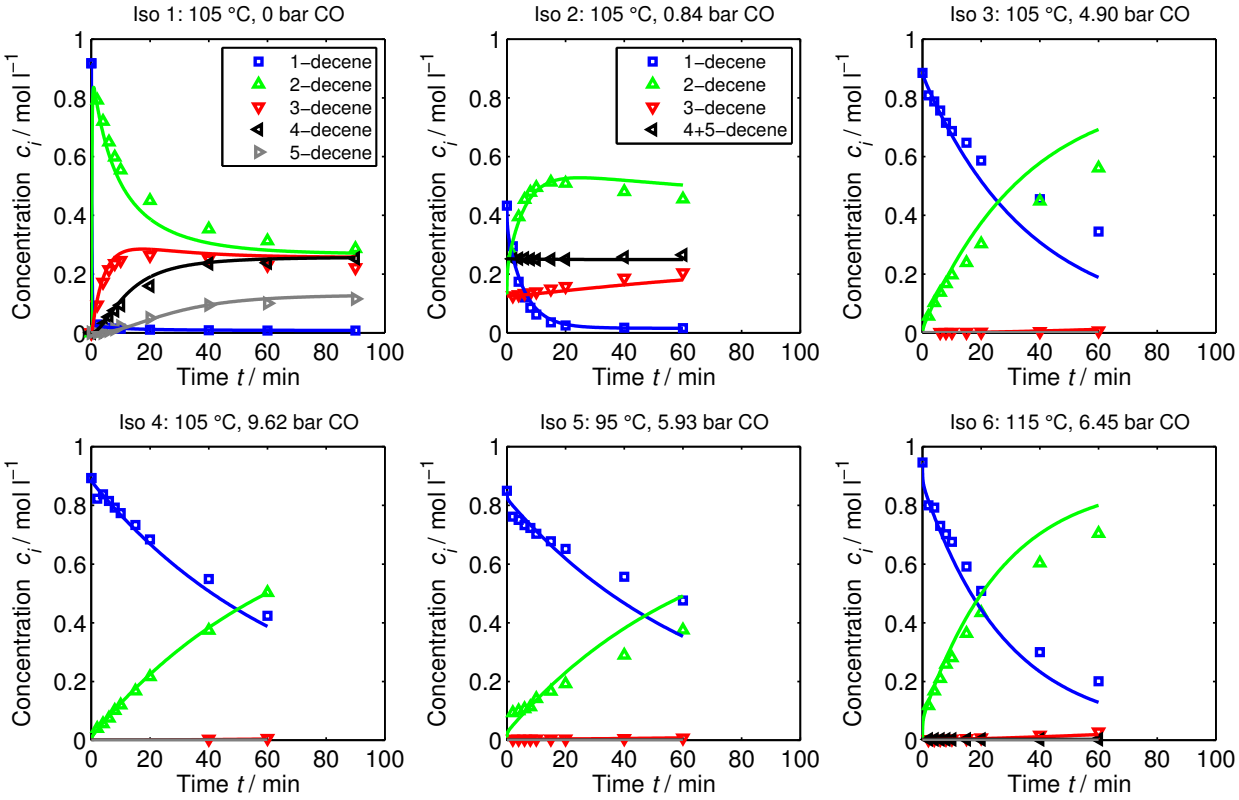

Figure 4: Experimental and modeling results of the isomerization network analysis. Symbols: Experimental data, Solid lines: Corresponding simulation using the developed mechanistic kinetic model. Legend in Iso 1 holds for all plots, except Iso 2. Experimental conditions: See table 1.

The recalculated apparent activation energies for the isomerization of 1-decene to 2-decene and all other isomerization reactions are 58.2 kJ mol^{-1} and 49.1 kJ mol^{-1}, respectively. These numbers are within the range of quantum chemical calculations for the isomerization of butenes and octenes with bulky Rh-diphosphine ligands ($\approx$ 40 - 80 kJ mol^{-1} at 125 °C) [48].

5.2. Hydrogenation

The experimentally determined and time resolved concentration profiles of the hydrogenation of 1-decene to decane (in accordance to table 1) are presented in figure 5 as well as the corresponding modeling results. In this analysis, the double bond isomerization is running in parallel to the hydrogenation. Because no CO is present in the hydrogenation experiments, the catalyst is always fully active and causes instant isomerization of 1-decene to internal decenes (Hyd 1). The hydrogenation reaction, however, appears to be slow compared to the isomerization. This can be explained by assuming that 1-decene is hydrogenated preferably because it has the least steric hindrances. Additionally, the low concentration

of 1-decene at equilibrium with the internal decenes causes a low driving force towards hydrogenation. Nevertheless, the hydrogenation proceeds and consumes 1-decene which disturbs the isomerization equilibrium. The double bond isomerization reaction works against this disturbance and restores the equilibrium which consumes the internal olefins (Hyd 2). In this sense, the hydrogenation is a tandem reaction as well as the tandem isomerization-hydroformylation discussed in section 2.

The mechanistic kinetic model represents the experimental data very well with only 3 estimated parameters for the hydrogenation (see table 2). Again, the assumption that the olefin coordination is the rate determining step for the hydrogenation as well is supported by the good fit of the model with experimental data. Representation of the coupled tandem character of the hydrogenation is achieved by modeling the simultaneously running isomerization reaction as equilibrium limited reaction that is able to run back and forth. The coupling element is the concentration of 1-decene because it gets consumed by hydrogenation and is refilled by the back-isomerization of internal olefins. It should be noted that the parameters that control the simultaneously running isomerization are the same as in the isomerization-only case shown in table 2. The recalculated apparent activation energy for the hydrogenation of 1-decene to decane is 64.2 kJ mol^{-1}, which is within a reasonable order of magnitude.

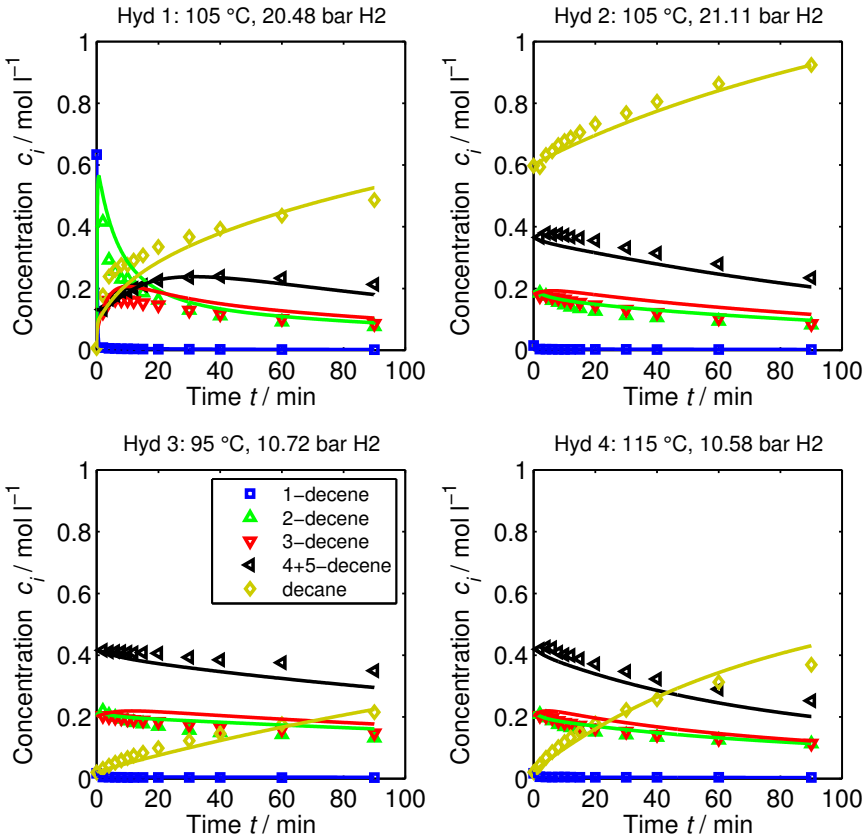

Figure 5: Experimental and modeling results of the hydrogenation network analysis. Symbols: Experimental data, Solid lines: Corresponding simulation using the developed mechanistic kinetic model. Legend in Hyd 3 holds for all plots. Experimental conditions: See table 1.

5.3. Hydroformylation

The experimentally determined and time resolved concentration profiles of the hydroformylation of 1-decene to undecanal (in accordance to table 1) are presented in figure 6 as well as the corresponding modeling results. The tandem isomerization-hydroformylation results are shown in figure 7. At this stage, all main and side reactions are running in parallel. During hydroformylation of terminal 1-decene (Hyfo 1-8), the double bond isomerization is the most severe side reaction. Especially at low synthesis gas pressures, the isomerization is dominating the yield (Hyfo 1), whereas the hydrogenation and the production of iso-aldehydes play always a minor role (Hyfo 7 zoom). Increasing the synthesis gas pressure from 6 bar (Hyfo 1) to 11 bar (Hyfo 2) and 22 bar (Hyfo 3) increases the aldehyde yield and the yield of undesired internal olefins drops because the isomerization is suppressed by CO. The conversion of 1-decene, however, is hardly affected by changing synthesis gas pressure.

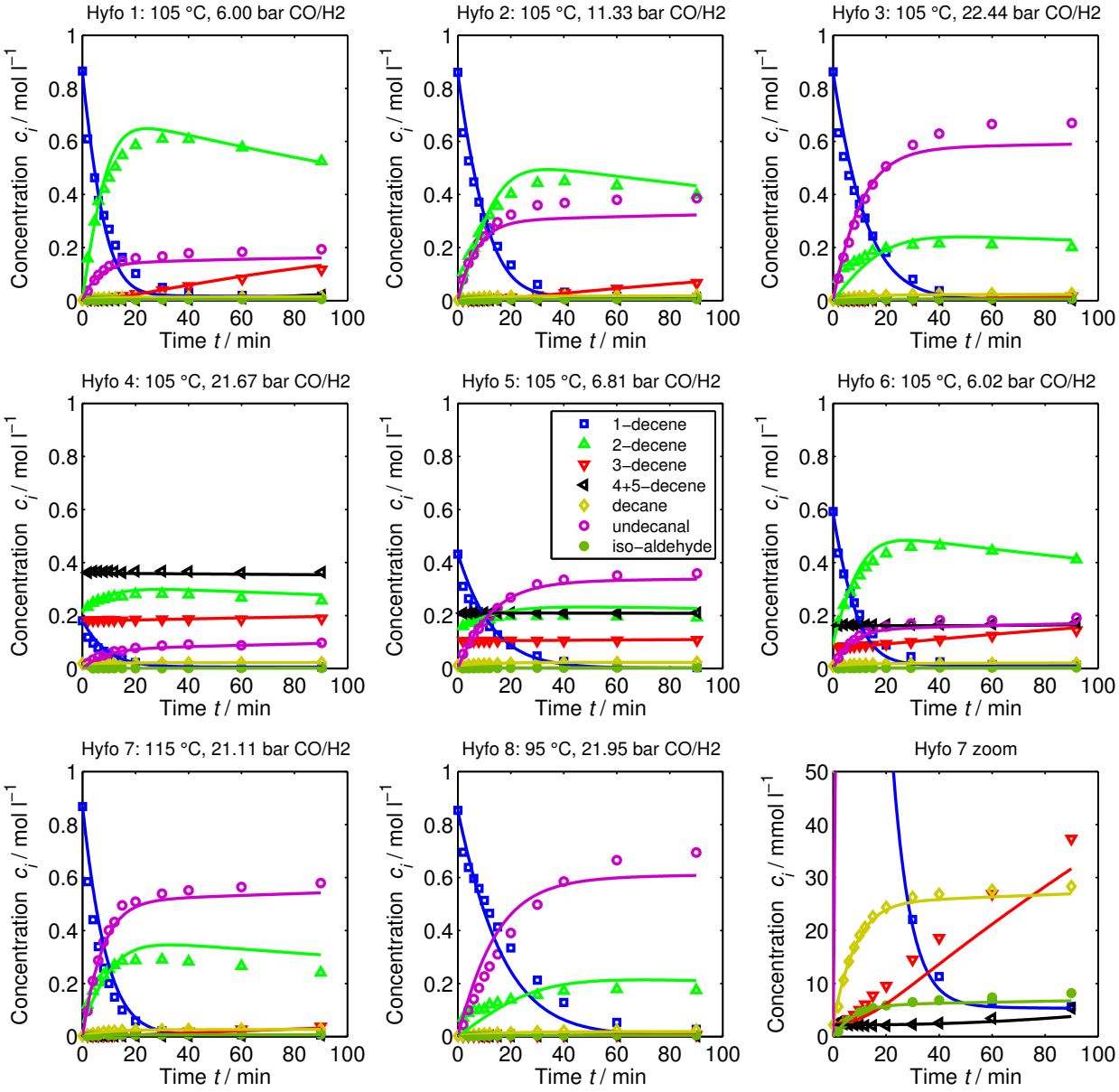

Figure 6: Experimental and modeling results of the hydroformylation network analysis. Symbols: Experimental data, Solid lines: Corresponding simulation using the developed mechanistic kinetic model. Legend in Hyfo 5 holds for all plots. Experimental conditions: See table 1.

Using mixtures of 1-decene and internal decenes (Hyfo 5) allows to overcome the low aldehyde yield with respect to 1-decene at low synthesis gas pressures. This is possible because the initially present concentration of internal decenes reduces the driving force of 1-decene isomerization. As a result, 1-decene undergoes hydroformylation to the desired aldehyde instead of being isomerized to undesired double bond isomers. This observation suggests recycling produced internal olefins in a continuous process to

substantially reduce the undesired double bond isomerization, if an isomerization active catalyst is used. The reaction temperature (Hyfo 7-8) has more influence on the isomerization than on the hydroformylation. Therefore, low reaction temperatures are required to increase the yield of the desired aldehyde and a lower apparent hydroformylation activation energy is expected compared to the isomerization. The temperature rise from 95 °C to 115 °C, however, hardly affected the linear:branched aldehyde ratio of 99:1.

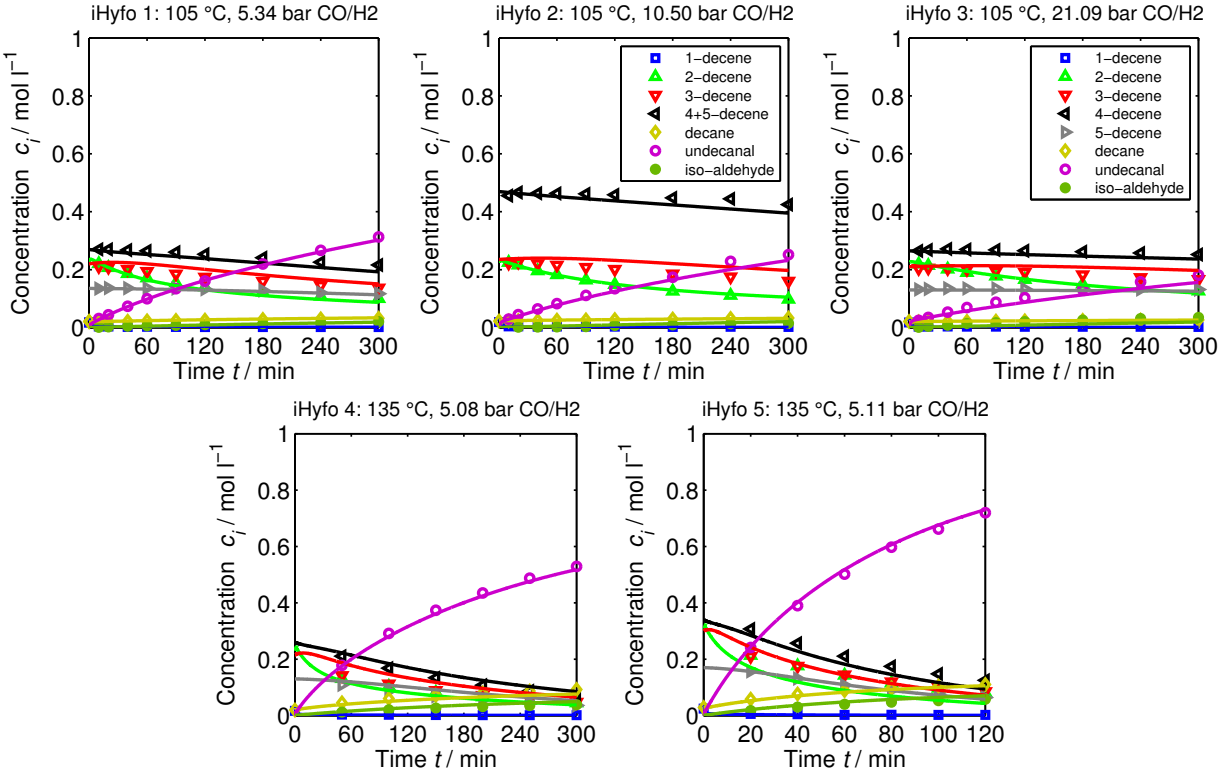

Figure 7: Experimental and modeling results of the tandem isomerization-hydroformylation network analysis. Symbols: Experimental data, Solid lines: Corresponding simulation using the developed mechanistic kinetic model. Legend in iHyfo 3 holds for all plots, except iHyfo2. Experimental conditions: See table 1.

In case of the tandem isomerization-hydroformylation, the pressure dependence trend observed for the hydroformylation of terminal 1-decene (Hyfo 1-3) is opposite compared to iHyfo 1-3. Surprisingly, the yield of the desired linear aldehyde decreases if the synthesis gas pressure is increased, although synthesis gas is a substrate. The explanation for this observation lies within the coupled nature of the tandem isomerization-hydroformylation, where the catalyst pre-equilibrium, the double bond isomerization and the hydroformylation reaction are connected via the concentration of dissolved CO. This coupling and its representation in the kinetic model is discussed in detail in section 6.

It was found experimentally that temperatures above 135 °C severely damage the catalyst [38]. Thus, the reaction temperature was increased to the maximum possible reaction temperature of 135 °C (iHyfo 4-5) to maintain fast hydroformylation as well as fast reproduction of consumed 1-decene by back-isomerization of internal decenes. This measure almost doubled the undecanal yield from 30 % (iHyfo 1) to 55 % (iHyfo 4). However, the linear:branched aldehyde ratio dropped at 135 °C to 93:7. In the last experiment (iHyfo 5), the catalyst loading was doubled additionally compared to iHyfo 4, which represents the optimized reaction conditions developed in [38]. Thus, it was possible to achieve a high product yield and productivity, similar to the hydroformylation of terminal 1-decene. However, twenty-times more catalyst was necessary compared to the hydroformylation of 1-decene which could be a drawback from an economic point of view. Nevertheless, the presented results encourage to perform tandem isomerization-hydroformylation reactions of long-chain olefins to produce valuable products with high selectivity and yield from less expensive but complex n-olefin isomer mixtures.

The mechanistic kinetic model represents the experimental hydroformylation and tandem isomerization-hydroformylation data very well with only 4 estimated parameters for each of the three hydroformylation rate laws presented in table 2. The recalculated apparent activation energy for the hydroformylation of 1-decene to undecanal (r_{hyfo1}) is 30.3 kJ mol^{-1}, whereas the production of iso-aldehydes ($r_{\mathrm{hyfo2-3}}$) showed an apparent activation energy of 56.7 kJ mol^{-1}, indicating that low reaction temperatures are beneficial for high n/iso selectivity. Only one parameter $\left(K^{\mathrm{IV}}_{\mathrm{hyfo}}\right)$ turned out to be insignificant and was finally excluded from the parameter estimation because it was estimated to be zero. It should be noted that at this stage all models of all side reactions run in parallel and that only one set of parameters is able to describe all borderline cases that have been studied experimentally. The assumption that the olefin coordination is the rate determining step is again supported by the good representation of all species by the model. Especially, the tandem case (iHyfo 1-5) can be described by the model with good quality as well as the hydroformylation of terminal 1-decene. Similar to the hydrogenation results, the equilibrium limited double bond isomerization reaction is the essential coupling element because it converts internal decenes to 1-decene which is consumed by hydroformylation.

The parity plots of all detected species in all experiments in figure 8 prove that no significant systematic errors are present in the model and that all deviations due to measurement noise are mostly within 20 %. This holds also for the side products (decane and iso-aldehyde, see Hyfo 7 zoom in figure 6) that appear in low concentrations during hydroformylation. Thus, the well-fitting mechanistic kinetic model is valid over a broad range of reaction conditions using a small number of estimated kinetic parameters.

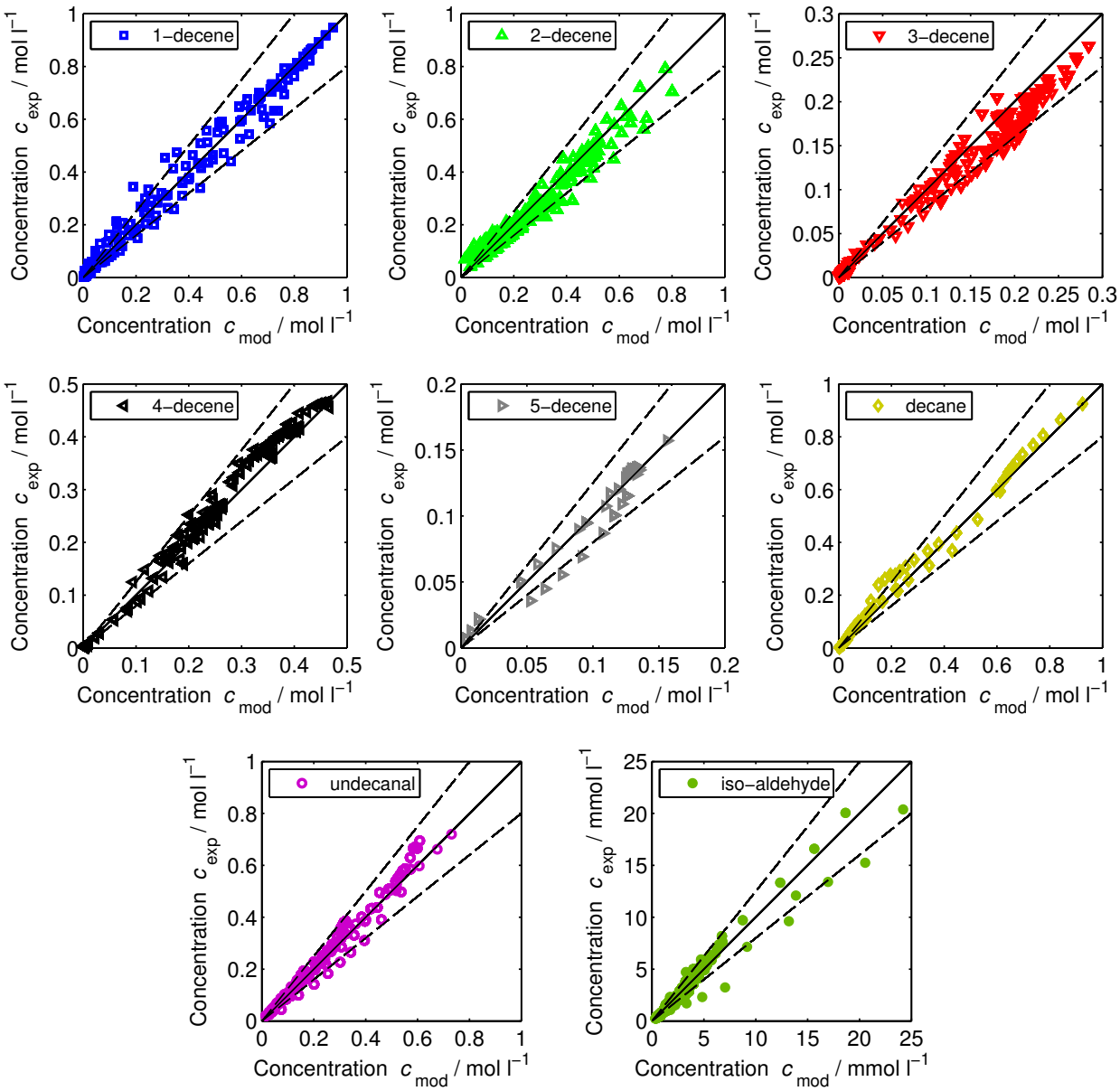

Figure 8: Parity plot of all detected species in all 23 performed kinetic experiments with 20 % deviation lines (dashed). Experimental conditions: See table 1

Table 2: Mechanistic kinetic models for the hydroformylation of 1-decene using a Rh-BiPhePhos catalyst, including side reactions and estimated kinetic parameter values with 95 % confidence interval. Temperature dependence of the rate constant is expressed as $k = \exp(A + B\,(1 - T_{\mathrm{ref}}/T))$, $T_{\mathrm{ref}} = 378$ K.

Model description	Equations, estimated parameters and 95 % confidence intervals
Catalyst resting state:	$c_{\mathrm{RS}} = \frac{c_{\mathrm{PC}}}{(1+K_{\mathrm{cat}}c_{\mathrm{CO}})}$ (5) $K_{\mathrm{cat}} = 5496.70\ \mathrm{l\ mol^{-1}} \pm 1.2\ \%$
Isomerization 1:	$r_{\mathrm{iso1}} = k_{\mathrm{iso1}}(T)\left(c_{\mathrm{1D}} - \frac{c_{\mathrm{2D}}}{K_{\mathrm{iso1}}}\right)c_{\mathrm{RS}}$ (13) $A_{\mathrm{iso1}} = 11.04 \pm 1.0\ \%\ \ B_{\mathrm{iso1}} = 18.53 \pm 8.5\ \%$ $K_{\mathrm{iso1}} = 33.77$ [19]
Isomerization 2:	$r_{\mathrm{iso2}} = k_{\mathrm{iso2}}(T)\left(c_{\mathrm{2D}} - \frac{c_{\mathrm{3D}}}{K_{\mathrm{iso2}}}\right)c_{\mathrm{RS}}$ (14) $A_{\mathrm{iso2}} = 6.94 \pm 1.4\ \%\ \ B_{\mathrm{iso2}} = 15.63 \pm 10.8\ \%$ $K_{\mathrm{iso2}} = 0.96$ [19]
Isomerization 3:	$r_{\mathrm{iso3}} = k_{\mathrm{iso3}}(T)\left(c_{\mathrm{3D}} - \frac{c_{\mathrm{4D}}}{K_{\mathrm{iso3}}}\right)c_{\mathrm{RS}}$ (15) $A_{\mathrm{iso3}} = 6.96 \pm\ 2.4\%\ \ B_{\mathrm{iso3}} = 15.63 \pm 10.8\ \%$ $K_{\mathrm{iso3}} = 1.00$ [19]
Isomerization 4:	$r_{\mathrm{iso4}} = k_{\mathrm{iso4}}(T)\left(c_{\mathrm{4D}} - \frac{c_{\mathrm{5D}}}{K_{\mathrm{iso4}}}\right)c_{\mathrm{RS}}$ (16) $A_{\mathrm{iso4}} = 5.96 \pm\ 3.3\%\ \ B_{\mathrm{iso4}} = 15.63 \pm 10.8\ \%$ $K_{\mathrm{iso4}} = 0.50$ [19]
Hydrogenation:	$r_{\mathrm{hyd}} = \frac{k_{\mathrm{hyd}}(T)c_{\mathrm{1D}}c_{\mathrm{H2}}c_{\mathrm{RS}}}{\left(1+K_{\mathrm{hyd}}c_{\mathrm{H2}}\right)}$ (17) $A_{\mathrm{hyd}} = 12.73 \pm\ 1.1\ \%\ \ B_{\mathrm{hyd}} = 20.44 \pm\ 7.4\ \%$ $K_{\mathrm{hyd}} = 10.20\ \mathrm{l\ mol^{-1}} \pm\ 17.4\ \%$
Hydroformylation 1:	$r_{\mathrm{hyfo1}} = \frac{k_{\mathrm{hyfo1}}(T)c_{\mathrm{1D}}c_{\mathrm{CO}}c_{\mathrm{H2}}c_{\mathrm{RS}}}{\left(1+K^{\mathrm{I}}_{\mathrm{hyfo}}c_{\mathrm{H2}}+K^{\mathrm{II}}_{\mathrm{hyfo}}c_{\mathrm{CO}}c_{\mathrm{H2}}\right)}$ (18) $A_{\mathrm{hyfo1}} = 20.41 \pm\ 1.0\ \%\ \ B_{\mathrm{hyfo1}} = 9.65 \pm\ 11.2\ \%$ $K^{\mathrm{I}}_{\mathrm{hyfo}} = 92.10\ \mathrm{l\ mol^{-1}} \pm\ 8.2\ \%$ $K^{\mathrm{II}}_{\mathrm{hyfo}} = 1063.60\ \mathrm{l^2\ mol^{-2}} \pm\ 4.0\ \%$
Hydroformylation 2:	$r_{\mathrm{hyfo2}} = \frac{k_{\mathrm{hyfo2}}(T)c_{\mathrm{1D}}c_{\mathrm{CO}}c_{\mathrm{H2}}c_{\mathrm{RS}}}{\left(1+K^{\mathrm{III}}_{\mathrm{hyfo}}c_{\mathrm{H2}}+K^{\mathrm{IV}}_{\mathrm{hyfo}}c_{\mathrm{CO}}c_{\mathrm{H2}}\right)}$ (19) $A_{\mathrm{hyfo2}} = 19.10 \pm\ 12.2\ \%\ \ B_{\mathrm{hyfo2}} = 18.04 \pm\ 9.2\ \%$ $K^{\mathrm{III}}_{\mathrm{hyfo}} = 5775.00\ \mathrm{l\ mol^{-1}} \pm\ 27.4\ \%$ $K^{\mathrm{IV}}_{\mathrm{hyfo}} \approx 0\ \mathrm{l^2\ mol^{-2}} \pm\ > 10^9\ \%$
Hydroformylation 3:	$r_{\mathrm{hyfo3}} = \frac{k_{\mathrm{hyfo3}}(T)c_{\mathrm{iD}}c_{\mathrm{CO}}c_{\mathrm{H2}}c_{\mathrm{RS}}}{\left(1+K^{\mathrm{III}}_{\mathrm{hyfo}}c_{\mathrm{H2}}+K^{\mathrm{IV}}_{\mathrm{hyfo}}c_{\mathrm{CO}}c_{\mathrm{H2}}\right)}$ (20) $A_{\mathrm{hyfo3}} = 14.90 \pm\ 15.9\ \%\ \ B_{\mathrm{hyfo3}} = 18.04 \pm\ 9.2\ \%$ $K^{\mathrm{III}}_{\mathrm{hyfo}} = 5775.00\ \mathrm{l\ mol^{-1}} \pm\ 27.4\ \%$ $K^{\mathrm{IV}}_{\mathrm{hyfo}} \approx 0\ \mathrm{l^2\ mol^{-2}} \pm\ > 10^9\ \%$

6. Model discussion

A high synthesis gas pressure means a high CO partial pressure which leads to a reduction of active catalyst concentration, represented by the catalyst resting state concentration c_{RS} in equation (5) (see figure 3). The isomerization reaction itself is not affected by CO but it is nevertheless inhibited strongly by CO because the reaction needs active catalyst. The hydroformylation reaction is driven by CO because it is a substrate but at the same time it is also inhibited by a decreasing catalyst resting state concentration. Furthermore, CO appears as inhibitor in the hydroformylation rate laws ((18) - (20)). The hydroformylation rate law (18) can be reformulated to discuss the dependence of the rate on the dissolved gases:

$$r_{\mathrm{hyfo1}} = \frac{k_{\mathrm{hyfo1}}(T) c_{\mathrm{1D}} c_{\mathrm{CO}} c_{\mathrm{H2}}}{\left(1 + K^{\mathrm{I}}_{\mathrm{hyfo}} c_{\mathrm{H2}}\right)\left(1 + \frac{K^{\mathrm{II}}_{\mathrm{hyfo}} c_{\mathrm{CO}} c_{\mathrm{H2}}}{1 + K^{\mathrm{I}}_{\mathrm{hyfo}} c_{\mathrm{H2}}}\right)} \cdot \frac{c_{\mathrm{PC}}}{(1 + K_{\mathrm{cat}} c_{\mathrm{CO}})}. \tag{21}$$

The isomerization reaction rates ((13) - (16)) are not influenced by dissolved H_2 and the apparent H_2 reaction order of the isomerization rate is always zero. The hydroformylation rate, however, is of course influenced by dissolved H_2 because it is a substrate. It can be seen from equation (21) that the hydroformylation rate will increase with increasing H_2 concentration until it a saturation regime is reached, similar to Michaelis-Menten or Eley-Rideal kinetics. Thus, the apparent H_2 hydroformylation reaction order decreases from a positive value to zero with increasing H_2 concentrations (see equation (22)) making it beneficial to operate the hydroformylation at high H_2 pressure.

$$r_{\mathrm{hyfo1}}(\text{high } c_{\mathrm{H2}}) \approx \frac{k^{*}_{\mathrm{hyfo1}}(T) c_{\mathrm{1D}} c_{\mathrm{CO}}}{\left(1 + K^{\mathrm{II}*}_{\mathrm{hyfo}} c_{\mathrm{CO}}\right)} \cdot \frac{c_{\mathrm{PC}}}{(1 + K_{\mathrm{cat}} c_{\mathrm{CO}})}. \tag{22}$$

The apparent hydroformylation reaction order of CO will also shift, starting at a positive value at low CO concentrations, passing zero and ending up at a negative value at very high CO concentrations (see equation (22)). This characteristic CO hydroformylation reaction order shift was also observed experimentally in the literature using different catalysts [49–55]. The isomerization, however, will always have a negative apparent reaction order with respect to CO.

In the coupled tandem case, the hydroformylation, which mostly consumes 1-decene, needs the isomerization reaction to reproduce the consumed 1-decene from internal decenes. Hence, it is beneficial for the tandem reaction to be operated at a certain low CO pressure to maintain a high hydroformylation rate as well as a high isomerization rate and it is obvious that an optimal CO pressure exists. The H_2 pressure also has an optimum which is a trade-off between hydroformylation and undesired hydrogenation. The

hydroformylation of terminal olefins, in turn, should be operated at high CO pressures to suppress undesired side reactions. Since these features are included in the developed mechanistic kinetic model, rigorous optimization was performed in the next section to find optimal reaction controls in terms of reaction temperature and pressure profiles for the hydroformylation and the tandem isomerization-hydroformylation case.

7. Optimal reaction control

Finding the optimal reaction conditions for the hydroformylation and the tandem isomerization-hydroformylation is not trivial because of the complex dependencies on the dissolved gases. Therefore, the developed and parameterized mechanistic kinetic model was taken to optimize a batch process for a maximized undecanal yield Y mathematically. It should be noted that it is intended with this study to find the optimal reaction temperature and pressure control profiles for the (tandem isomerization-)hydroformylation to illustrate how the optimal reaction conditions evolve over reaction time. However, a realization of these controls can be very challenging, especially for a industrially more relevant continuous production process. The used batch reactor model, the gas solubilities and mass transfer coefficients were taken from [31]. To compare both, hydroformylation and the tandem reaction, an initial total olefin concentration of 1 mol l^{-1} was fixed for both cases as well as a typical space time yield STY for hydroformylation reactors of 100 kg m^{-3} h^{-1} aldehyde product [56]. The degrees of freedom for the optimization are the reaction temperature and the partial pressures of CO and H_2 within the experimentally validated range as time functions. The resulting optimal control problem (23) was solved by transformation of the problem into a high dimensional nonlinear program NLP by discretization of the resulting differential and algebraic equations with orthogonal collocation on finite elements [57–59].

AMPL in combination with the conopt 3.17A solver was used for all optimization calculations [60].

$$\text{Obj} = \max_{T(t),p_{CO}(t),p_{H_2}(t)} Y_{\text{undecanal}}\left(t_{\text{end}}\right) \tag{23}$$

s.t.

Balance equations - [31]

Gas solubilities - [31]

Mass transfer coefficients - [31]

Kinetic model - this work

$STY = 100\ \text{kg m}^{-3}\ \text{h}^{-1}$

The optimization results for the hydroformylation of 1-decene are shown in figure 9. As expected, the reaction temperature is at the lower boundary of 95 °C and the partial pressures of CO and H_2 are at the upper boundary of 10 bar (total synthesis gas pressure = 20 bar), initially. This is a result of the already discussed temperature and pressure dependencies and aims for the suppression of the undesired olefin isomerization. At high conversion of 1-decene, the temperature is increased to the upper limit of 135 °C to increase the low hydroformylation rate because of the low 1-decene concentration. Furthermore, the CO partial pressure is reduced to 1 bar and less to increase the amount of active catalyst while the H_2 partial pressure remains at the upper boundary of 10 bar. This represents a change of the reaction to tandem mode (see drop of 2-decene in figure 10-a) with an optimal low CO pressure, as discussed in section 6. The maximum achievable yield of undecanal for the hydroformylation of 1-decene at the specified STY is 82 %.

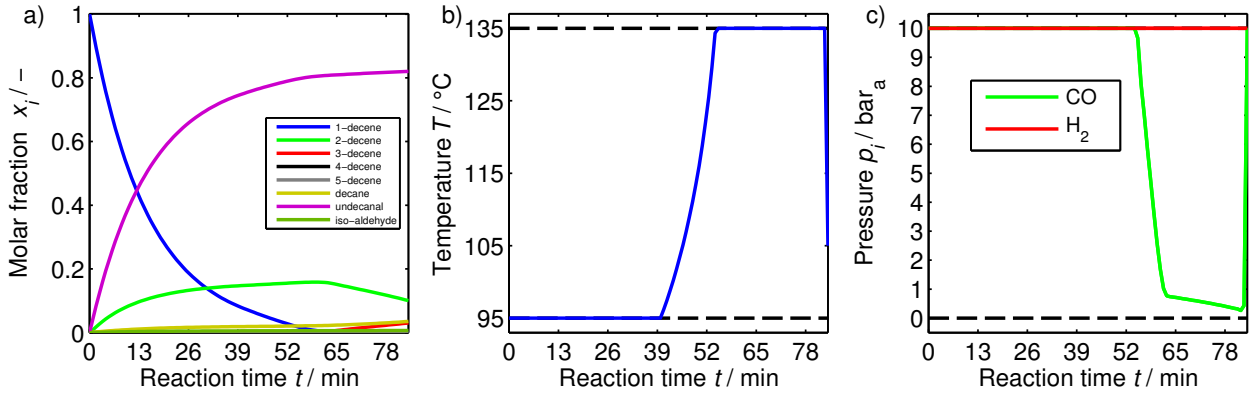

Figure 9: Optimization results for the hydroformylation of 1-decene. Rh:Olefin = 1:10000. STY = 100 kg m^{-3} h^{-1} a) Concentration profiles in molar fraction. b) Optimal temperature profile. c) Optimal partial pressure profiles.

The optimization results for the tandem isomerization-hydroformylation of internal decenes are shown in figure 10. The optimal temperature profile is always constant at the upper boundary of 135 °C to keep the hydroformylation rate high. The isomerization is also fast in reproducing consumed 1-decene from the internal decenes. As expected by the discussion in section 6, the optimal CO pressure profile is always at low values and drops almost linearly from 2.5 bar to 0.5 bar. The drop in CO pressure compensates the decreasing substrate concentrations by increasing the active amount of catalyst. The H_2 pressure also follows an optimal trajectory between 5 and 10 bar. Keeping the H_2 pressure at the upper limit would result in more hydrogenation and less aldehyde yield whereas a low H_2 pressure would reduce the hydroformylation rate. The increase of the H_2 pressure at the end of the reaction to the upper limit increases the hydroformylation rate and compensates the low substrate concentration to meet the desired STY.

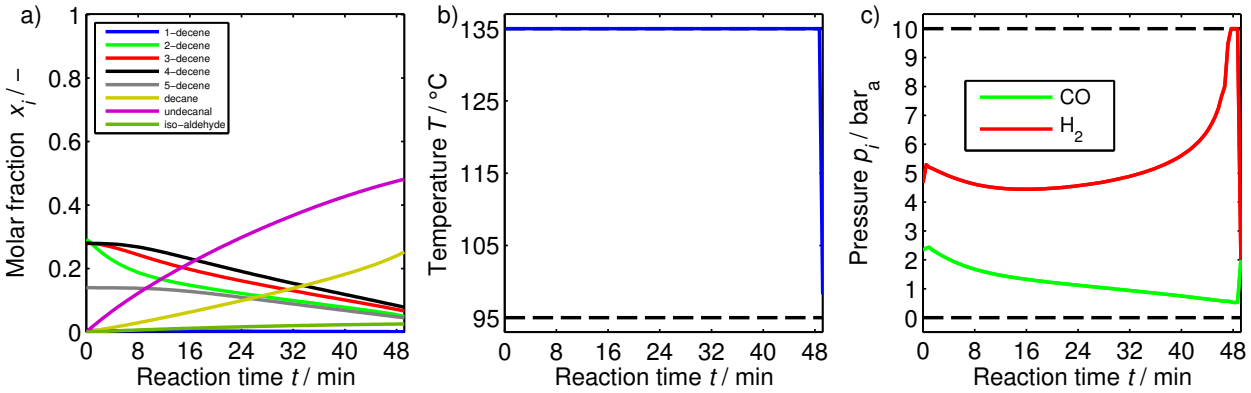

Figure 10: Optimization results for the tandem isomerization-hydroformylation of internal decenes. Rh:Olefin = 1:500. STY = 100 kg m^{-3} h^{-1} a) Concentration profiles in molar fraction. b) Optimal temperature profile. c) Optimal partial pressure profiles.

The maximum yield of undecanal for the tandem isomerization-hydroformylation of internal decenes at the specified STY is 48 %. In this case, also significant amounts of decane are produced by hydrogenation with a yield of 25 %. The amount of byproducts (decane, iso-aldehydes) can be reduced if a lower STY is acceptable because the temperature and H_2 partial pressure can be reduced (see figure 11). For example, if a STY of only 25 kg m^{-3} h^{-1} is required, the maximum achievable aldehyde yield increases up to 83 % and the decane yield decreases down to 10 % because of the lower temperature and H_2 pressure (see figure 11-b and c). On the other hand, this results in more reaction time or residence time (reactor volume) compared to conventional hydroformylation reactors and more solvent and catalyst hold up which would be a drawback in terms of invest costs. Therefore, a cost optimization would be necessary to find the optimal reaction control for a production case but this scenario is beyond the scope of this contribution.

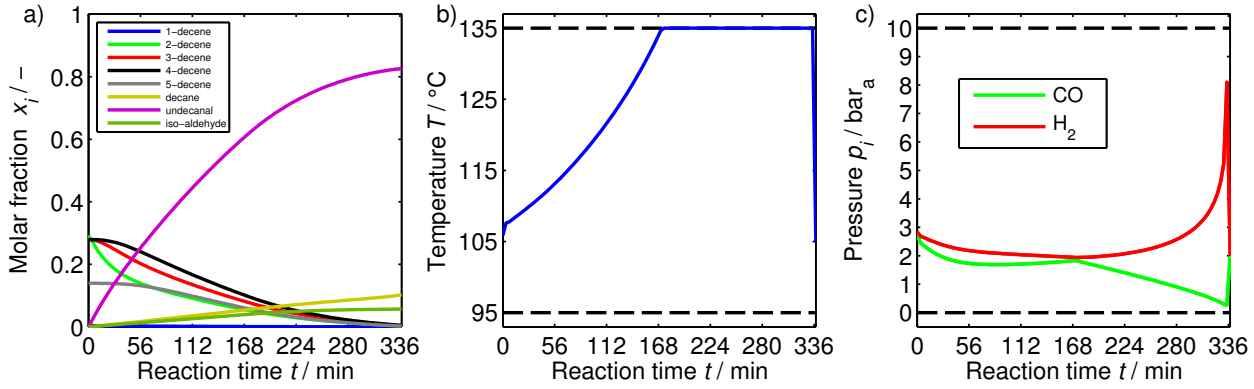

Figure 11: Optimization results for the tandem isomerization-hydroformylation of internal decenes. Rh:Olefin = 1:500. STY = 25 kg m^{-3} h^{-1} a) Concentration profiles in molar fraction. b) Optimal temperature profile. c) Optimal partial pressure profiles.

8. Summary and conclusion

In this contribution, the Rh-BiPhePhos catalyzed hydroformylation and tandem isomerization-hydroformylation of n-decenes was investigated experimentally and by theoretical modeling. The complex reaction network included several side reactions, such as double bond isomerization, hydrogenation and the production of undesired iso-aldehydes. It was possible, to decouple and study the complex reaction system in 23 well planned isomerization, hydrogenation and hydroformylation experiments separately by manipulating the initial concentrations of the reactants and the gas phase compositions during the reactions. A mechanistic kinetic model based on an extended reaction mechanism including all main and side reactions was developed. It was fitted to the experimental data with low deviation between model and experiment. The estimated kinetic parameters were within reasonable orders of magnitude and showed low 95 % confidence intervals. Special emphasis was given to the tandem isomerization-hydroformylation reaction of internal decenes to undecanal, which could also be described by the model in all studied cases with very low deviations. It turned out that the reversible isomerization reaction of terminal 1-decene to internal decenes is essential, because it couples the internal olefins via 1-decene to the production of undecanal. Interestingly, it was found that the tandem reaction obeys an opposite pressure dependence compared to the conventional hydroformylation of 1-decene. It was possible to describe these features with the developed kinetic model as well as all borderline cases of the hydroformylation of 1-decene and internal decenes to undecanal. The observed trends are a consequence of the complex interactions between the CO induced catalyst deactivation, the isomerization and the hydroformylation reaction. These findings lead to the conclusion that the hydroformylation of terminal olefins should be operated at high synthesis gas pressure and low temperature to suppress undesired

side reactions such as double bond isomerization. The tandem isomerization-hydroformylation, however, should be performed at low synthesis gas pressure and high temperature for a maximized productivity of the desired linear aldehyde, although the linear:branched aldehyde ratio decreases with increasing reaction temperature. These strategies could be confirmed by calculating optimal control profiles for reaction temperature and pressures. In conclusion, the developed kinetic model builds the basis for an efficient process design. Furthermore, the modeling strategy can be transferred to more challenging tandem isomerization-hydroformylation reactions of green feedstocks such as oleochemicals with internal double bond.

Acknowledgment

The financial support of the German Science Foundation (Project SFB/TRR 63: "InPROMPT - Integrated Chemical Processes in Multi-Phase Fluid Systems") for this joint collaboration (Subprojects A1/A3) is gratefully acknowledged. We are also very grateful to Umicore AG and Co. KG for the supply of the catalyst precursor Rh(acac)$(CO)_2$.

Appendix

A. Local parameter subset selection

Estimating kinetic parameters of the mechanistic kinetic model requires that these parameters are identifiable. This question can be answered by calculating the rank of the Fisher Information Matrix FIM which corresponds to the number of identifiable model parameters [61]. The FIM is calculated from the parameter sensitivity matrix S (see equation (A.1)) which represents the derivatives of the measured states of the model y with respect to the kinetic parameters θ. Additional QR-decomposition of the FIM reveals the sensitive parameter subset that can be identified and estimated [62, 63]. Since the states of the model are time dependent under (semi)batch conditions, the FIM and the rank are also time dependent. Therefore, it is possible that kinetic model parameters lose their identifiability or become identifiable after a certain reaction time which requires a time resolved rank analysis of the FIM (known as local parameter subset selection). Details about the derivation of the local analysis, the underlying (semi)batch reactor model and gas solubilities can be found in the literature [31].

$$FIM = S^{\mathrm{T}} S = \left(\frac{\partial y_i}{\partial \theta_j}\right)^{\mathrm{T}} \left(\frac{\partial y_i}{\partial \theta_j}\right) \tag{A.1}$$

The numerical rank of the $FIM(t)$ is determined by the number of condition numbers $\kappa(t)$ that are less than a numerical threshold (see equation (A.2)). Calculating $\kappa(t)$ requires a singular value decomposition of the matrix at every time point into singular values $\sigma(t)$ which can be done numerically using built-in Matlab functions (svd). The numerical threshold depends on the number of model parameters N_θ and the square root of the machine precision ε.

$$\kappa_i(t) = \frac{\sigma_{\max}(t)}{\sigma_i(t)} < \frac{1}{N_\theta \sqrt{\varepsilon}} \tag{A.2}$$

The results of the local parameter subset selection analysis of the presented kinetic models in table 2 with respect to the experimental design summarized in table 1 is shown in figure A.1. It is clearly visible that the condition numbers for all subnetwork analyses are strongly time dependent. However, it was possible to keep all condition numbers below the numerical threshold by the experimental design of the network analysis which means that all kinetic model parameters are identifiable and can be estimated. From this analysis follows that the sensitive parameter subset is identical to the set of kinetic parameters.

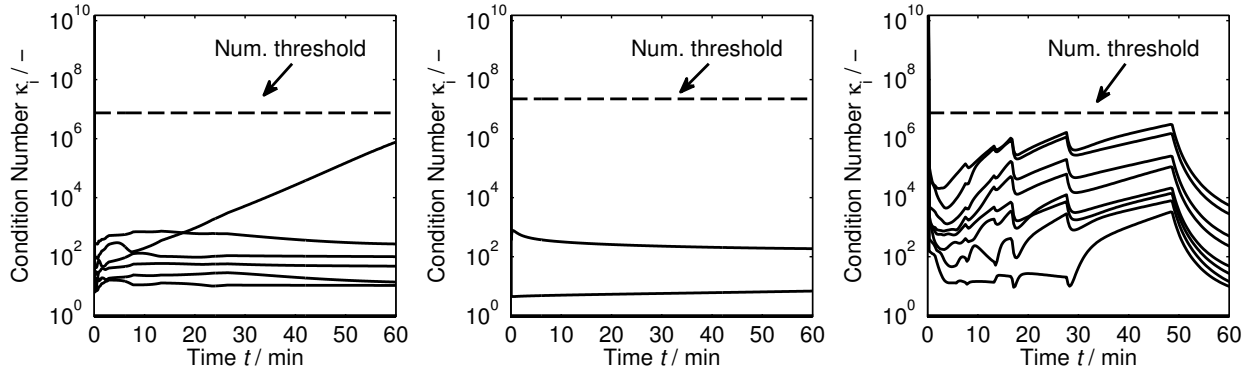

Figure A.1: Time resolved condition numbers of the *FIM* for the reaction subnetwork analysis. From left to right: Isomerization, hydrogenation and (tandem isomerization-)hydroformylation (see table 1).

Nomenclature

Abbreviations

BP	BiPhePhos
cat	Catalyst
CI	Confidence interval
CO	Carbon monoxide
1D	1-decene
iD	Internal n-decene
dmf	N,N-dimethylformamide
dod	n-dodecane
FID	Flame ionization detector
GC	Gas chromatograph
H_2	Molecular hydrogen
HDC	hydridodicarbonyl
Hyd	Hydrogenation
Hyfo	Hydroformylation
iHyfo	Tandem isomerization-hydroformylation
Iso	Isomerization
PC	Precursor
rel	Relative
Rh	Rhodium
RS	Resting state
svd	Singular value decomposition
TMS	Thermomorphic multicomponent solvent system
ve	Valence electrons

Indices

i, j	component index

Constants

R	gas constant	$8.3145\,\mathrm{J\,mol^{-1}\,K^{-1}}$

Latin Symbols

A	Reformulated rate constant
B	Reformulated activation energy
$\mathbb{C}$	Christiansen matrix
c	Concentration in $\mathrm{mol\,l^{-1}}$
E_A	Activation energy in $\mathrm{J\,mol^{-1}}$
FIM	Fisher information matrix
K	Equilibrium / inhibition constant
k	Rate constant
N	Number
n	Number of elementary steps
p	Pressure in bar
r	Reaction rate in $\mathrm{mol\,l^{-1}\,min^{-1}}$
S	Sensitivity matrix
T	Temperature in K
t	Time in min
y	Model state

Greek Symbols

ε	Machine precision
κ	Condition number
λ	Pseudo first order rate coefficient
ν	Stoichiometric number
σ	Singular value
θ	Model parameter

References

[1] R. Franke, D. Selent, A. Börner, Applied hydroformylation, Chem. Rev. 112 (11) (2012) 5675–5732.

[2] A. Behr, P. Neubert, Applied homogeneous catalysis, Wiley-VCH, Weinheim, 2012.

[3] M. Beller, A. Renken, R. van Santen, Catalysis: From principles to applications, Wiley-VCH, Weinheim, 2012.

[4] D. Evans, J. Osborn, G. Wilkinson, Hydroformylation of alkenes by use of rhodium complex catalysts, J. Chem. Soc. A (1968) 3133–3142.

[5] M. Kranenburg, Y. van der Burgt, P. Kamer, P. van Leeuwen, K. Goubitz, J. Fraanje, New diphosphine ligands based on heterocyclic aromatics inducing very high regioselectivity in rhodium-catalyzed hydroformylation: Effect of the bite angle, Organometallics 14 (6) (1995) 3081–3089.

[6] P. Kamer, P. van Leeuwen, J. Reek, Wide bite angle diphosphines: Xantphos ligands in transition metal complexes and catalysis, Acc. Chem. Res. 34 (11) (2001) 895–904.

[7] C. Kunze, D. Selent, I. Neda, M. Freytag, P. Jones, R. Schmutzler, W. Baumann, A. Börner, Calix[4]arene-based bis-phosphonites, bis-phosphites, and bis-O-acyl-phosphites as ligands in the rhodium(I)-catalyzed hydroformylation of 1-octene, Z. Anorg. Allg. Chem. 628 (4) (2002) 779–787.

[8] D. Selent, W. Baumann, R. Kempe, A. Spannenberg, D. Röttger, K.-D. Wiese, A. Börner, Reactions of a hydroxy phosphonite ligand in the coordination sphere of rhodium(I), Organometallics 22 (21) (2003) 4265–4271.

[9] R. van Eldik, S. Aygen, H. Kelm, A. Trzeciak, J. Ziólkowksi, Kinetic and spectroscopic studies of the substitution reactions of $[Rh(acac)(CO)_2]$ with triphenylphosphite, Transition Met. Chem. 10 (1985) 167–171.

[10] E. Billig, A. Abatjoglou, D. Bryant, US patent 4668651 A: Polyphosphite complex hydroformylation catalyst (1987).

[11] B. Moasser, W. Gladfelter, D. Roe, Mechanistic aspects of a highly regioselective catalytic alkene hydroformylation using a rhodium chelating bis(phosphite) complex, Organometallics 14 (8) (1995) 3832–3838.

[12] A. van Rooy, E. Orij, P. Kamer, P. van Leeuwen, Hydroformylation with a rhodium/bulky phosphite modified catalyst. A comparison of the catalyst behavior for oct-1-ene, cyclohexene, and styrene, Organometallics 14 (1) (1995) 34–43.

[13] P. van Leeuwen, P. Kamer, J. Reek, P. Dierkes, Ligand bite angle effects in metal-catalyzed C-C bond formation, Chem. Rev. 100 (8) (2000) 2741–2770.

[14] C. Vogl, E. Paetzold, C. Fischer, U. Kragl, Highly selective hydroformylation of internal and terminal olefins to terminal aldehydes using a rhodium-BIPHEPHOS-catalyst system, J. Mol. Catal. A: Chem. 232 (1-2) (2005) 41–44.

[15] E. Schäfer, Y. Brunsch, G. Sadowski, A. Behr, Hydroformylation of 1-dodecene in the thermomorphic solvent system dimethylformamide/decane. Phase behavior - reaction performance - catalyst recycling, Ind. Eng. Chem. Res. 51 (31) (2012) 10296–10306.

[16] J. Markert, Y. Brunsch, T. Munkelt, G. Kiedorf, A. Behr, C. Hamel, A. Seidel-Morgenstern, Analysis of the reaction network for the Rh-catalyzed hydroformylation of 1-dodecene in a thermomorphic multicomponent solvent system, Appl. Catal. A 462-463 (2013) 287–295.

[17] G. Kiedorf, D. Hoang, A. Müller, A. Jörke, J. Markert, H. Arellano-Garcia, A. Seidel-Morgenstern, C. Hamel, Kinetics of 1-dodecene hydroformylation in a thermomorphic solvent system using a rhodium-biphephos catalyst, Chem. Eng. Sci. 115 (2014) 31–48.

[18] A. Rost, Y. Brunsch, A. Behr, R. Schomäcker, Comparison of the activity of a rhodium-biphephos catalyst in thermomorphic solvent mixtures and microemulsions, Chem. Eng. Tech. 37 (6) (2014) 1055–1064.

[19] A. Jörke, A. Seidel-Morgenstern, C. Hamel, Isomerization of 1-decene: Estimation of thermodynamic properties, equilibrium composition calculation and experimental validation using a Rh-BIPHEPHOS catalyst, Chem. Eng. J. 260 (2015) 513–523.

[20] A. Jörke, E. Kohls, S. Triemer, A. Seidel-Morgenstern, C. Hamel, M. Stein, Resolution of structural isomers of complex reaction mixtures in homogeneous catalysis, Chem. Eng. Process. Process Intensif. 102 (2016) 229–237.

[21] A. Jess, P. Wasserscheid, Chemical technology: An integral textbook, Wiley-VCH, Weinheim, 2013.

[22] P. van Leeuwen, C. Claver, Rhodium catalyzed hydroformylation, Vol. 22 of Catalysis by metal complexes, Kluwer Academic Publishers, Dordrecht and Boston, 2000.

[23] A. Behr, D. Obst, C. Schulte, T. Schosser, Highly selective tandem isomerization-hydroformylation reaction of trans-4-octene to n-nonanal with rhodium-BIPHEPHOS catalysis, J. Mol. Catal. A: Chem. 206 (1-2) (2003) 179–184.

[24] A. Behr, D. Obst, B. Turkowski, Isomerizing hydroformylation of trans-4-octene to n-nonanal in multiphase systems: Acceleration effect of propylene carbonate, J. Mol. Catal. A: Chem. 226 (2) (2005) 215–219.

[25] M. Vilches-Herrera, L. Domke, A. Börner, Isomerization-hydroformylation tandem reactions, ACS Catal. 4 (6) (2014) 1706–1724.

[26] E. Frankel, Selective hydroformylation of unsaturated fatty acid esters, Ann. N.Y. Acad. Sci. 214 (1) (1973) 79–93.

[27] A. Behr, D. Obst, A. Westfechtel, Isomerizing hydroformylation of fatty acid esters: Formation of ω-aldehydes, Eur. J. Lipid Sci. Technol. 107 (4) (2005) 213–219.

[28] A. Behr, A. Westfechtel, J. Pérez Gomes, Catalytic processes for the technical use of natural fats and oils, Chem. Eng. Tech. 31 (5) (2008) 700–714.

[29] A. Behr, A. Vorholt, Hydroformylation and related reactions of renewable resources, in: M. Meier, B. Weckhuysen, P. Bruijnincx (Eds.), Organometallics and Renewables, Vol. 39 of Topics in Organometallic Chemistry, Springer, Berlin and Heidelberg, 2012, pp. 103–127.

[30] T. Vanbésien, E. Monflier, F. Hapiot, Hydroformylation of vegetable oils: More than 50 years of technical innovation, successful research, and development, Eur. J. Lipid Sci. Technol. 118 (1) (2016) 26–35.

[31] A. Jörke, S. Triemer, A. Seidel-Morgenstern, C. Hamel, Kinetic investigation exploiting local parameter subset selection: Isomerization of 1-decene using a Rh-Biphephos catalyst, Chem. Ing. Tech. 87 (6) (2015) 713–725.

[32] A. Jörke, A. Seidel-Morgenstern, C. Hamel, Rhodium-biphephos catalyzed hydroformylation studied by operando FTIR spectroscopy: Catalyst activation and rate determining step, J. Mol. Catal. A: Chem., in press doi:10.1016/j.molcata.2016.10.028.

[33] M. Garland, P. Pino, Kinetics of the formation and hydrogenolysis of acylrhodium tetracarbonyl, Organometallics 10 (6) (1991) 1693–1704.

[34] R. Deshpande, Effect of pH on rate and selectivity behavior in biphasic hydroformylation of 1-octene, J. Mol. Catal. A: Chem. 126 (2-3) (1997) 133–140.

[35] R. Jennerjahn, I. Piras, R. Jackstell, R. Franke, K.-D. Wiese, M. Beller, Palladium-catalyzed isomerization and hydroformylation of olefins, Chem. Eur. J. 15 (26) (2009) 6383–6388.

[36] A. Behr, Technische Konzepte zum Recycling von Homogenkatalysatoren, Chem. Ing. Tech. 70 (6) (1998) 685–695.

[37] A. Behr, C. Fängewisch, Temperature-dependent multicomponent solvent systems - An alternative concept for recycling homogeneous catalysts, Chem. Eng. Tech. 25 (2) (2002) 143–147.

[38] T. Gaide, A. Jörke, K. Schlipköter, C. Hamel, A. Seidel-Morgenstern, A. Behr, A. Vorholt, Isomerization / hydroformylation tandem reaction of a decene isomeric mixture with subsequent catalyst recycling in thermomorphic solvent systems, Appl. Catal. A, submitted and available for review.

[39] J. Christiansen, The elucidation of reaction mechanisms by the method of intermediates in quasi-stationary concentrations, Vol. 5 of Advances in Catalysis, Elsevier, 1953, pp. 311–353.

[40] O. Levenspiel, Chemical reaction engineering, 3rd Edition, Wiley, New York, 1999.

[41] F. Helfferich, Kinetics of multistep reactions, 2nd Edition, Vol. 40 of Comprehensive chemical kinetics, Elsevier, Amsterdam and Boston, 2004.

[42] D. Murzin, T. Salmi, Catalytic kinetics, Elsevier, Amsterdam, 2005.

[43] P. Kamer, A. van Rooy, G. Schoemaker, P. W. van Leeuwen, In situ mechanistic studies in rhodium catalyzed hydroformylation of alkenes, Coord. Chem. Rev. 248 (21-24) (2004) 2409–2424.

[44] M. Shaharun, B. Dutta, H. Mukhtar, S. Maitra, Hydroformylation of 1-octene using rhodium-phosphite catalyst in a thermomorphic solvent system, Chem. Eng. Sci. 65 (1) (2010) 273–281.

[45] M. Schwaab, J. Pinto, Optimum reference temperature for reparameterization of the arrhenius equation. Part 1: Problems involving one kinetic constant, Chem. Eng. Sci. 62 (10) (2007) 2750–2764.

[46] M. Schwaab, L. Lemos, J. Pinto, Optimum reference temperature for reparameterization of the arrhenius equation. Part 2: Problems involving multiple reparameterizations, Chem. Eng. Sci. 63 (11) (2008) 2895–2906.

[47] C. Kubis, D. Selent, M. Sawall, R. Ludwig, K. Neymeyr, W. Baumann, R. Franke, A. Börner, Exploring between the extremes: Conversion-dependent kinetics of phosphite-modified hydroformylation catalysis, Chem. Eur. J. 18 (28) (2012) 8780–8794.

[48] M. Carvajal, S. Kozuch, S. Shaik, Factors controlling the selective hydroformylation of internal alkenes to linear aldehydes. 1. The isomerization step, Organometallics 28 (13) (2009) 3656–3665.

[49] P. Purwanto, H. Delmas, Gas-liquid-liquid reaction engineering: Hydroformylation of 1-octene using a water soluble rhodium complex catalyst, Catal. Today 24 (1-2) (1995) 135–140.

[50] R. Deshpande, P. Purwanto, H. Delmas, R. Chaudhari, Kinetics of hydroformylation of 1-octene using $[Rh(COD)Cl]_2$-TPPTS complex catalyst in a two-phase system in the presence of a cosolvent, Ind. Eng. Chem. Res. 35 (11) (1996) 3927–3933.

[51] M. Diwakar, R. Deshpande, R. Chaudhari, Hydroformylation of 1-hexene using Rh/TPPTS complex exchanged on anion exchange resin: Kinetic studies, J. Mol. Catal. A: Chem. 232 (1-2) (2005) 179–186.

[52] V. Srivastava, S. Sharma, R. Shukla, N. Subrahmanyam, R. Jasra, Kinetic studies on the hydroformylation of 1-hexene using $RhCl(AsPh_3)_3$ as a catalyst, Ind. Eng. Chem. Res. 44 (6) (2005) 1764–1771.

[53] M. Rosales, A. González, Y. Guerrero, I. Pacheco, R. Sánchez-Delgado, Kinetics and mechanisms of homogeneous catalytic reactions, J. Mol. Catal. A: Chem. 270 (1-2) (2007) 241–249.

[54] A. Sharma, C. Lebigue, R. Deshpande, A. Kelkar, H. Delmas, Hydroformylation of 1-octene using [Bmim][PF_6]-decane biphasic media and rhodium complex catalyst: Thermodynamic properties and kinetic study, Ind. Eng. Chem. Res. 49 (21) (2010) 10698–10706.

[55] R. Deshpande, A. Kelkar, A. Sharma, C. Julcour-Lebigue, H. Delmas, Kinetics of hydroformylation of 1-octene in ionic liquid-organic biphasic media using rhodium sulfoxantphos catalyst, Chem. Eng. Sci. 66 (8) (2011) 1631–1639.

[56] M. Beller, Catalytic carbonylation reactions, Vol. 18 of Topics in Organometallic Chemistry, Springer, Berlin, 2006.

[57] S. Oh, R. Luus, Use of orthogonal collocation method in optimal control problems, Int. J. Control 26 (5) (1977) 657–673.

[58] L. Biegler, Solution of dynamic optimization problems by successive quadratic programming and orthogonal collocation, Comput. Chem. Eng. 8 (3-4) (1984) 243–247.

[59] J. Logsdon, L. Biegler, Accurate solution of differential-algebraic optimization problems, Ind. Eng. Chem. Res. 28 (11) (1989) 1628–1639.

[60] AMPL - A mathematical programming language v3.1.1.201602042304 (2016).
URL `http://www.ampl.com`

[61] G. Franceschini, S. Macchietto, Model-based design of experiments for parameter precision: State of the art, Chem. Eng. Sci.

63 (19) (2008) 4846–4872.

[62] T. Barz, D. López Cárdenas, H. Arellano-Garcia, G. Wozny, Experimental evaluation of an approach to online redesign of experiments for parameter determination, AIChE J. 59 (6) (2013) 1981–1995.

[63] M. Fink, A. Attarian, H. Tran, Subset selection for parameter estimation in an HIV model, Proc. Appl. Math. Mech. 7 (1) (2007) 1121501–1121502.